Laboratory for Atmospheric and Space Physics
University of Colorado
Boulder, Colorado

South African National Space Agency
Hospital Street, Hermanus 7200, South Africa

Earth Observing System
SOlar Radiation and Climate Experiment
(EOS SORCE)

Algorithm Theoretical Basis Document – Post Launch update

Solar Stellar Irradiance Comparison Experiment (SOLSTICE)

Document No. 164787 Date: April 22, 2021

Description/Summary/Contents:

In this document we describe the scientific basis of the Level-1 processor algorithms used for the Solar Stellar Irradiance Comparison Experiment (SOLSTICE), flying on the SORCE platform. This document represents an update to the pre-launch ATBD that was reviewed and published April 2000 and applies specifically to the algorithms developed and/or refined to support post launch processing.

Prepared by Martin Snow, William McClintock, Joshua Elliott, Blake Vanier, Emma Lieb, and Vanessa George Date April 22, 2021

Approved by Thomas Woods Date April 22, 2021

Revisions				
Rev	Description of Change	By	Approved	Date

Table of Contents

1. INTRODUCTION

1.1. Purpose of this Document

The original and this updated Algorithm Theoretical Basis Document (ATBD) describe the algorithms used to produce all data levels of solar spectral irradiance for the SORCE SOLar-STellar Irradiance Comparison Experiment (SOLSTICE) instrument. This document provides the scientific motivation and goal of the SORCE mission, a brief introduction to the SOLSTICE instrument and a detailed discussion of the updated algorithms utilized in the production of scientific results since the original SORCE ATBD. It is not designed to serve as the only reference to the SORCE SOLSTICE instrument, data, and its algorithms. The original SORCE ATBD, SOLSTICE reference papers (see Section 1.3), and other related documents should be consulted to complement the information contained here.

1.2. Scope

This document describes the updated algorithms required to generate solar spectral data sets from direct observations of the Sun by the SORCE SOLSTICE instrument. The updated algorithms are described as they are known for the final SOLSTICE data product archive in 2020.

1.3. Applicable Documents

The applicable documents since the original SORCE ATBD are the SOLSTICE reference papers listed in Table 1.1. These papers are about its design, calibration, and data products.

McClintock, W., Rottman, G., & Woods, T. (2005a) Solar-stellar irradiance comparison experiment II (SOLSTICE II): instrument concept and design, Solar Physics, 230, 225	SOLSTICE design
McClintock, W., Snow, M., & Woods, T. (2005b) Solar-stellar irradiance comparison experiment II (SOLSTICE II): pre-launch and on-orbit calibrations, Solar Physics, 230, 259	SOLSTICE calibration
Snow, M., McClintock, W., Rottman, G., & Woods, T. (2005a) Solar-stellar irradiance comparison experiment II (SOLSTICE II): examination of the solar stellar comparison technique, Solar Physics, 230, 295	Description of in-flight degradation correction algorithm
Snow, M., et al. (2005b) The Mg II index from SORCE, Solar Physics, 230, 325	Description of algorithm to produce MgII index from SOLSTICE and SIM
Snow, M., et al. (2013) A new catalog of ultraviolet stellar spectra for calibration, in *Cross-Calibration of Far UV Spectra of Solar System Objects and the Heliosphere*, E. Quémerais, M. Snow, and R-M. Bonnet (eds), ISSI Scientific Report Series volume 13, pp 191	Validation of calibration in stellar mode

Snow, M., et al. (2014) Comparison of magnesium II core-to-wing ratio observations during solar minimum 23/24	Modification of original algorithm for MgII
Snow, M., et al. (2019) A revised magnesium II core-to-wing ratio from SORCE SOLSTICE, Earth & Space Science, 11, 2106	Final update to MgII algorithm for SORCE SOLSTICE

1.4. Contributing Authors

Martin Snow	SORCE SOLSTICE Instrument Scientist
William E. McClintock	SORCE SOLSTICE Instrument Scientist
Joshua Elliott	SORCE SOLSTICE Data System Lead
Blake Vanier	SORCE Data Systems
Emma Lieb	SORCE Data Systems
Thomas N. Woods	SORCE Principal Investigator
Laura Sandoval	SORCE Archive Lead

2. OVERVIEW and BACKGROUND INFORMATION

2.1. Introduction

The Sun is the dominant direct energy source to the Earth's climate system. The majority of the total solar irradiance (TSI) is transmitted through Earth's atmosphere and deposits most of its energy at Earth's surface. Many of the solar ultraviolet (UV) wavelengths are deposited in Earth's atmosphere. Figure 1 shows the altitude of optical depth unity as a function of wavelength over the range measured by SOLSTICE (115-300 nm). The far ultraviolet (FUV; 115-200 nm) is absorbed in the thermosphere and mesosphere, while the middle ultraviolet (MUV; 200-300 nm) deposits its energy in the stratosphere. Over the solar cycle, the FUV varies by more than 10%, with some wavelengths such as Lyman alpha varying by 60%. The solar cycle variation of the MUV is generally only a few percent, but the Mg II lines near 280 nm change by more than 10%.

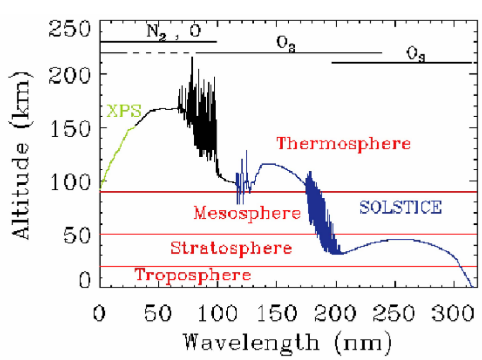

Figure 1. Energy deposition from far ultraviolet solar spectral irradiance in the atmosphere. The ranges indicated along the top of the plot show the dominant atmospheric constituent responsible for absorption at those wavelengths.

2.2. Science and Mission Goals and Objectives

The overall goal of SORCE is the measurement of solar irradiance and the specification of its variability with high accuracy, precision and stability, for global change applications. The specific science objectives that must be accomplished in order to achieve the goal are comprehensive, and address issues including measurement accuracy, spectral coverage and resolution, temporal resolution, and the timeliness of the data delivery to the scientific community. See the SORCE pre-flight ATBD document for the complete list of SORCE Level 1 science objectives and mission goals. For SOLSTICE, SORCE makes a daily SSI measurement to produce its Level 3 data product of the entire wavelength range. Additional data products over smaller wavelength ranges at higher time cadence are also available.

2.3. SOLSTICE Instrument Description

The primary goal for the SORCE mission is the specification of solar total and spectral irradiance and its variability with high accuracy, precision and stability. To achieve this goal, and the associated science objectives, the SORCE mission consists of five separate optical devices — one four-channel cavity radiometer called the Total Irradiance Monitor (TIM); three spectrometers, one called the Solar Irradiance Monitor (SIM) and two (redundant) copies of the Solar Stellar Irradiance Comparison Experiment (SOLSTICE); and one photometer array called the X-ray ultraviolet Photometer System (XPS). Only SOLSTICE is discussed in this document. SOLSTICE is a scanning grating monochrometer (McClintock et al. 2005a) that measures the 115-300 nm wavelength range. It has a spectral resolution of 0.1 nm in solar mode, and uses photomultiplier tubes (PMT) as the detectors. There are two SOLSTICE instruments on SORCE, referred to as SOLSTICE A and SOLSTICE B. Each SOLSTICE is identical, having both FUV and MUV detector channels. At any one time, only one detector channel is active, although the other detector (inactive channel) is also read out at the same cadence as the active channel. The inactive channel is used in data processing as described in Sections 4.3.1.1 and 4.3.2.2. SOLSTICE has two modes, solar and stellar. In solar mode, the entrance aperture is a 0.1x0.1 mm square. The stellar entrance aperture is a 16 mm diameter circle. A bi-stable mechanism switches between the two. A separate mechanism switches between two exit slits for the two modes. The stellar mode is one of the primary means for maintaining on-orbit calibration.

Heritage for SORCE SOLSTICE comes from the SOLSTICE instrument on the Upper Atmosphere Research Satellite (UARS, Rottman et al. 1993).

3. ALGORITHM DESCRIPTION

3.1. Physics of the Problem

Converting detector signals into solar irradiance units is a direct calculation as described in McClintock et al. (2005b). Photons are converted to electrons by the PMT photocathode, amplified by the PMT dynode chain, and read out by the electronics. The instrument was calibrated before flight at NIST SURF III. Instrument degradation is corrected through observations of bright stars and measurements over the field-of-view and is validated through comparisons of on-board redundant SOLSTICE A and B instruments

3.2. Conversion from Instrument Signal to Irradiance

McClintock et al. (2005b) provides the details of the measurement equation for SOLSTICE. Solar irradiance (E) in units of W/m^2/nm is determined from the measured count rate (C) and the preflight and inflight calibrations. Equations 1 and 2 show the basic calculation used in the data processing system. The solar irradiance is the primary science data product from SOLSTICE.

3.2.1. Measurement Equation

$$E_{AU}(\lambda) = \frac{C(\lambda,\ \tau,\ D_C,\ Sl,\ St)}{R_C(\lambda,\ T,\ \Omega) FOV(\lambda,\ \Omega,\ \theta,\ \phi) A_{Entrance} \Delta\lambda_{BP} T_{Filter}(\lambda) DEG(t, \lambda,\ \Omega,\ \theta,\ \phi) f_{AU}} \quad (1)$$

.

$$C(\lambda,\ \tau,\ Dc,\ Sl,\ St) = \frac{S(\lambda)N(\tau) - Dc - Sl(\lambda) - St}{\Delta t} \quad (2)$$

3.2.1.1. Explanation of Terms

Measured count rates are corrected for detector nonlinearity (N), dark rate (D), scattered and stray light (Sl and St). Equation 2 has been modified since its description in McClintock et al. (2005b) and will be described in Section 4.2. This corrected count rate is then divided by the preflight responsivity at the center of the FOV (R_c), a pointing correction (FOV), the area of the entrance aperture (A), the spectral bandpass (Δλ), transmission of the filter combination (T), degradation (DEG), and a correction to a standard 1 astronomical unit (f_{AU}). DEG is determined from the stellar measurements, FOV is determined from cruciform alignments during the primary mission and from offpoint spectral scans during Day Only Operations (DO-Op).

Term in Measurement Equation	Meaning	Units	Origin
E_{AU}	SSI corrected to 1 AU as a function of wavelength	W/m^2/nm	Data Product
C	Corrected Count Rate	counts/s	Measured
R_C	Center point responsivity		Preflight
FOV	Correction for pointing	Unitless	Inflight
$A_{Entrance}$	Area of entrance aperture	m^2	Preflight
$\Delta\lambda_{BP}$	Bandpass	Nm	Preflight
T_{Filter}	Filter transmission	Unitless	Inflight
DEG	Degradation correction	Unitless	Inflight

f_{AU}	Correction to 1 AU	Unitless	Calculated/inflight
S(lambda)	Observed signal	Counts	Measured
N	Nonlinearity as a function of dead time, tau		Inflight
D_c	Dark current	Counts	Inflight
Sl(lambda)	Scattered Light	Photons	Inflight
St	Stray light	Photons	Inflight
Delta t	Integration time	s	Preflight
T	Temperature	C	Measured
Ω, θ, φ	Solid angle, pitch, yaw	radians	Measured
τ	Detector dead time	ns	Preflight/Inflight

4. CALIBRATION and INSTRUMENT CHARACTERIZATION

4.1. Overview of Pre-flight Calibrations

The SURF calibration is described in McClintock et al. (2005b). The primary calibration was at the NIST Synchrotron Ultraviolet Radiation Facility (SURF). Validation of the calibration using standard stars is described in Snow et al. (2013).

4.2. Operational Changes from Original ATBD

4.2.1. Overview of Observations

During the first three years of the mission, the operational mode was that during the solar period of the orbit, SOLSTICE A measured the MUV spectrum while SOLSTICE B measured the FUV spectrum. Once per week, the two instruments would be cross-calibrated with an "ABComparison" activity. In addition to normal spectral scans in both directions, several orbits per day were devoted to calibration observations: fixed wavelength for the whole orbit, mini-scans of selected spectral features to measure wavelength stability, weekly filter transmission calibrations, and weekly cruciform alignment scans to measure shifts in the bore sight and to also measure the solar-stellar field of view correction (FOV).

During the eclipse period of each orbit, both SOLSTICEs would measure stellar irradiances. The two instruments would alternate between FUV and MUV on a daily basis. They would also observe "dark" regions of the sky, i.e. regions free of UV-bright objects, in order to track detector dark rates. These observations were frequently corrupted by the South Atlantic Anomaly (SAA). The increased background level from the SAA did not saturate the detectors, so the strength and position of the SAA could be measured over the mission.

In January 2006, there was an anomaly with the entrance aperture mechanism on SOLSTICE A (Section 4.2.2). After the anomaly, SOLSTICE A was placed in solar mode for the remainder of the mission. Only SOLSTICE B continued to make stellar observations after that.

Due to the degradation of the SORCE batteries, SOLSTICE A was powered off during eclipses starting in 2009. In 2010, SOLSTICE B was also powered off during eclipses. The factor DEG in the measurement equation was extrapolated for the rest of the mission for the MUV channel.

Late in the mission, several FUV stellar spectra were taken (Section 4.4.1). At this time, the ABComparison cross-calibration activities were made daily instead of weekly.

In late 2011, a battery anomaly caused the spacecraft to be in safe hold for six weeks. When operations resumed, a much smaller number of instrument activities were allowed. In particular, cruciform alignment scans were no longer possible, so the measurements used to determine the solar/stellar field-of-view correction ceased. There were additional battery anomalies with the more severe one in July 2013. New mission operation strategies had to be developed, called the Day Only Operations (DO-Op) mode, whereby the spacecraft can be powered off during orbit eclipse. The temperature variations for the instruments vary much more in this DO-Op mode than they did previously. SOLSTICE was still able to make >90% of its planned solar observations. There is a six month gap for SORCE solar observations in late 2013 to early 2014 while developing flight software for this DO-Op mode.

There have been a few stellar and cruciform scans made near the end of the mission to provide some validation of the long term trends. Following adequate overlap with the TSIS-1 solar irradiance observations, the SORCE observations ended on February 25, 2020.

4.2.2. In-flight Anomalies

SOLSTICE A has had one major anomaly. In January 2006, coming out of eclipse, the commands to put the entrance aperture back into solar mode did not activate the mechanism. For several minutes, the instrument was pointed at the Sun with the stellar aperture. When the mechanism finally activated, the entrance aperture did not come to rest in exactly the same position as it had before the anomaly. This introduced a wavelength shift which has been taken into account by the data processing system thereafter. After this event, SOLSTICE A remained in solar mode and its stellar observations ceased. Only SOLSTICE B continued to make stellar measurements.

4.2.2.1. One-day Hits

SOLSTICE B also had one major anomaly. In July 2006, it observed the Sun with the stellar aperture in place for an entire solar period. There was a measurable loss of MUV responsivity as shown in Figure 2. The detector responsivity recovered over the next several months. We used the SOLSTICE A observations over this short time period to correct for the rapidly changing SOLSTICE B responsivity. The behavior of SORCE SOLSTICE under these circumstances was very similar to the behavior of UARS SOLSTICE to similar anomalies. Several additional anomalies of this type have also been identified later in the mission, but none were as severe as the July 2006 event.

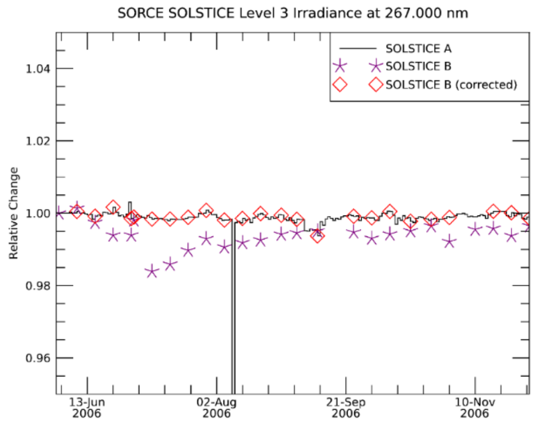

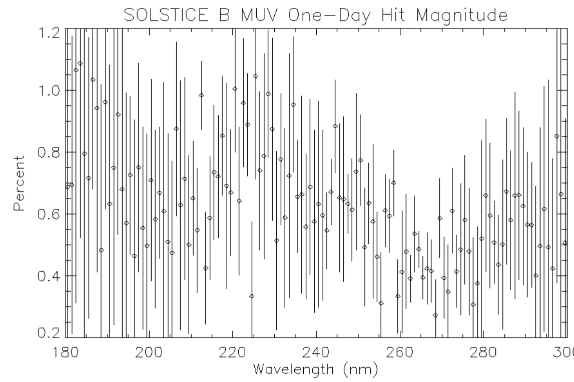

Figure 2. Short term changes in MUV responsivity due to an operational anomaly that exposed the instrument to the Sun with the stellar aperture.

Figure 3 shows the correction for the July 2006 one-day hit in the FUV. Even though the instrument was in FUV mode, so the FUV detector was exposed, the magnitude of the change in responsivity was quite small. A reasonable assumption is that the exposure of the optics to the full solar flux caused the change. The MUV channel also saw some recovery over the next few months.

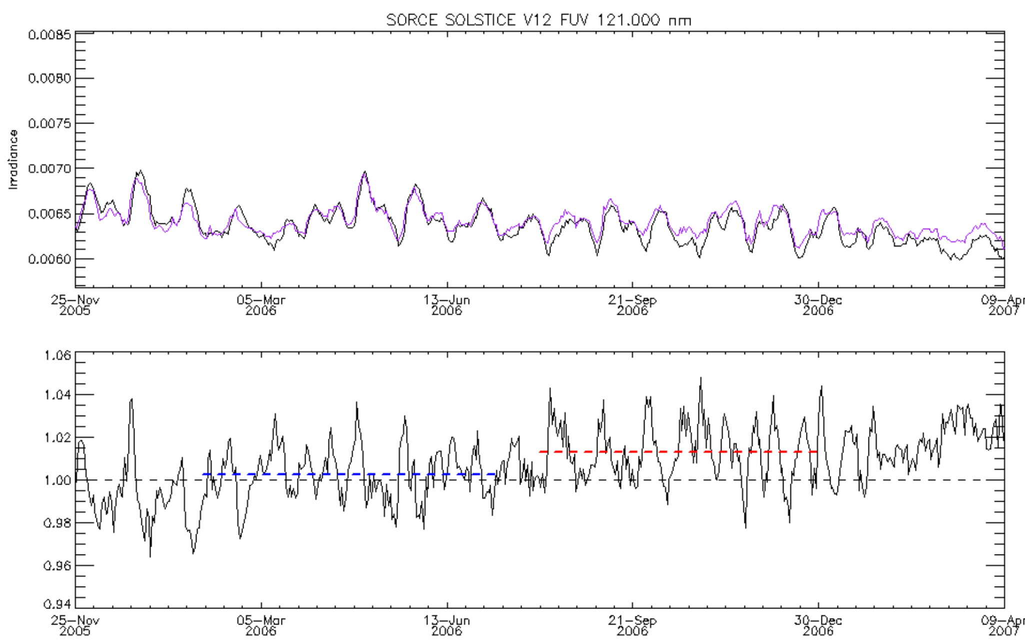

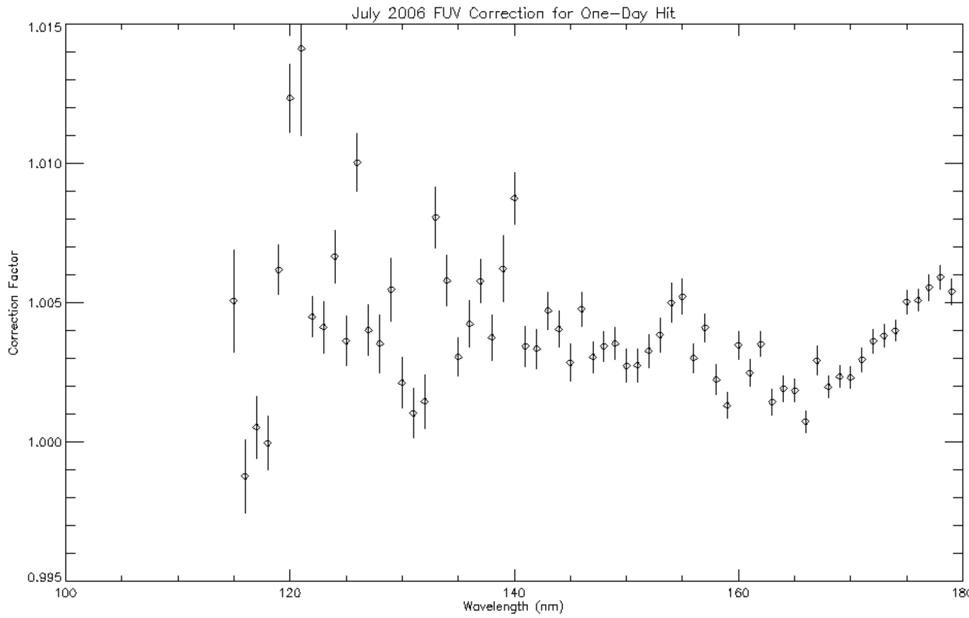

Figure 3. (top) time series of FUV irradiances showing a discontinuity the time of the anomaly. The black curve is the NRLSSI2 Lyman alpha irradiance, purple is the uncorrected SOLSTICE irradiance. The middle panel shows the ratio as a function of time. The average before the anomaly is shown by the blue dashed line, while the average ratio after the anomaly is shown by the red dashed line. The magnitude of the change in the ratio is shown in lower panel along with an estimate of the uncertainty in this correction. It is larger than 1% at Lyman alpha, but much closer to 0.5% for other FUV wavelengths.

4.2.2.2. The Vacation ("spike" correction)

The other anomaly that had a significant effect was the long safehold event in 2013. The degradation of the battery caused the entire spacecraft to be put in safehold from July 2013 until February 2014 (The Vacation). During this long period at low temperature, the responsivity of the instrument changed by several percent. Since there is no calibration data during the vacation, and no absolute stellar observations before or afterwards, we have had to resort to using a calibrated irradiance model to estimate the change in responsivity over the six-month gap. We compare the relative change in the NRLSSI2 (Coddington et al. 2016) model before and after the safehold event, and then apply this ratio to the SOLSTICE data after the vacation. This method does not change the long-term trending in SOLSTICE. It only applies the change in irradiance over the safehold event. Figure 4 shows the time series of SOLSTICE data with and without the correction at a single wavelength. Figure 5 shows the magnitude of this correction as a function of wavelength.

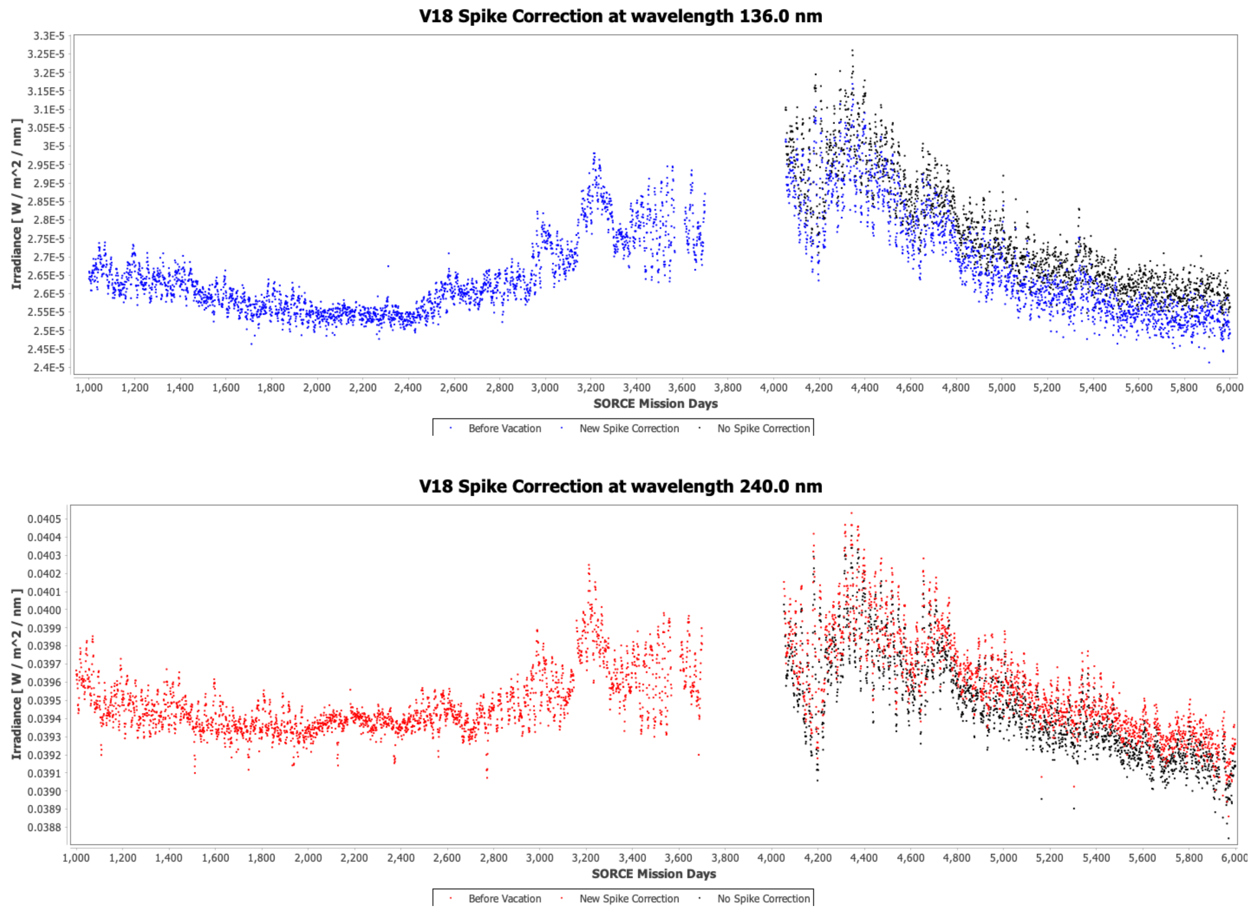

Figure 4. Time series of SOLSTICE daily average irradiances spanning the vacation. (top) FUV irradiances at 136 nm and (bottom) MUV irradiances at 240 nm. Both plots show the irradiance with and without the correction.

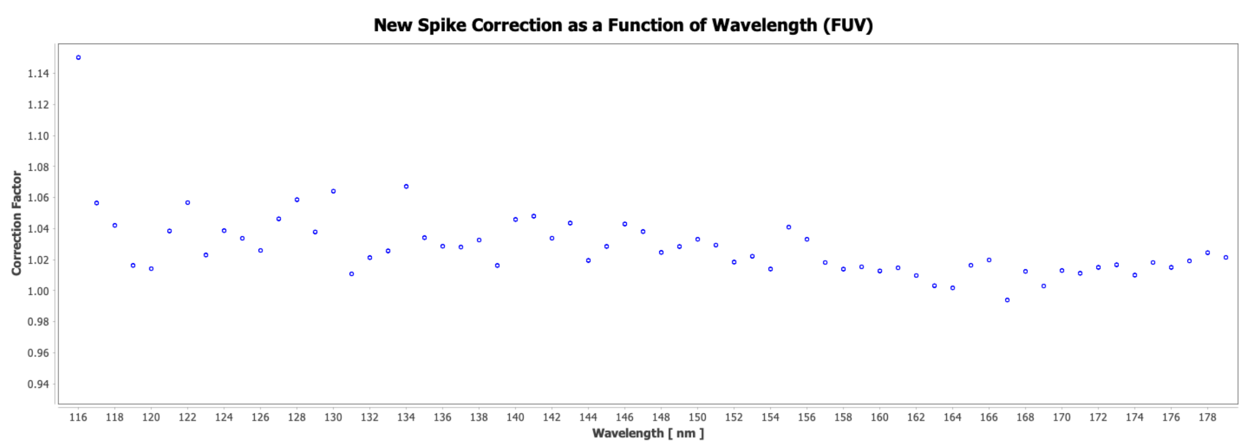

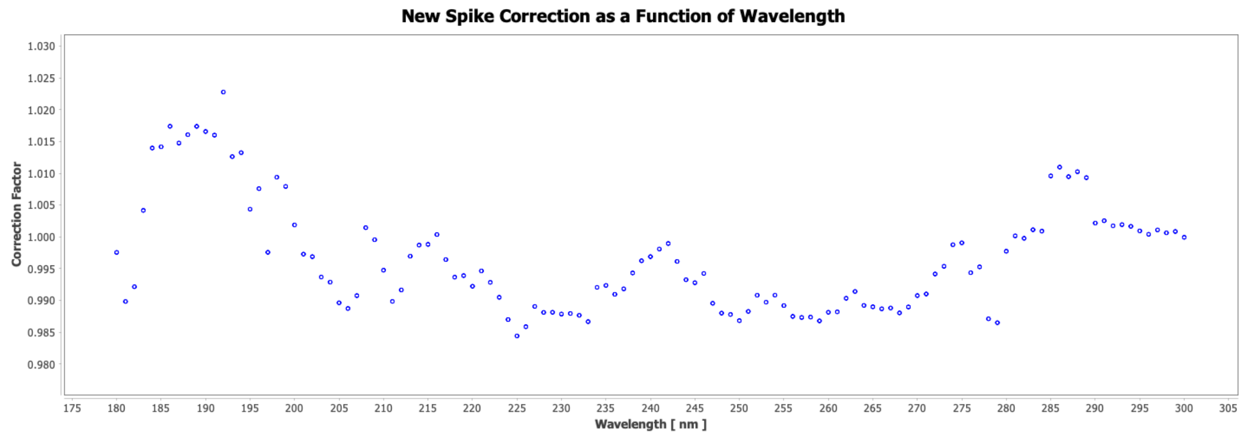

Figure 5. Magnitude of the responsivity change during the safehold event for FUV and MUV channels.

The "spike" correction is currently being updated and uncertainty estimates will go into the version 18 data product.

4.2.2.3. GCI Lockups

Shortly after launch, it was discovered that the Generic Channel Interfaces (GCI) for all instruments would lock up after passage through the South Atlantic Anomaly (SAA). The effect was that no housekeeping data would be telemetered to the ground. The solution was to add a telemetry monitor (TMON) that would check to see if the housekeeping data stream was stale. If so, the instrument would be power cycled. This TMON activated at the beginning of each solar period so that the data loss would be less than one orbit.

4.3. Flight Calibrations

4.3.1. Standard Calibrations

4.3.1.1. Dark

The dark rate for both MUV channels was significantly higher on orbit than it had been on the ground during preflight testing. Not only was the count rate higher, it also changed over time. The dark rate for the two FUV channels was similar to preflight levels, and has been stable over the mission. Figure 6 shows the dark rates for the four channels over the mission. The dark rates are collected during ABComparison experiments. These experiments measure both FUV and MUV during a single orbit. The count rate observed by the inactive channel is averaged over the orbit. The dark rate used in data processing is a smooth function of time.

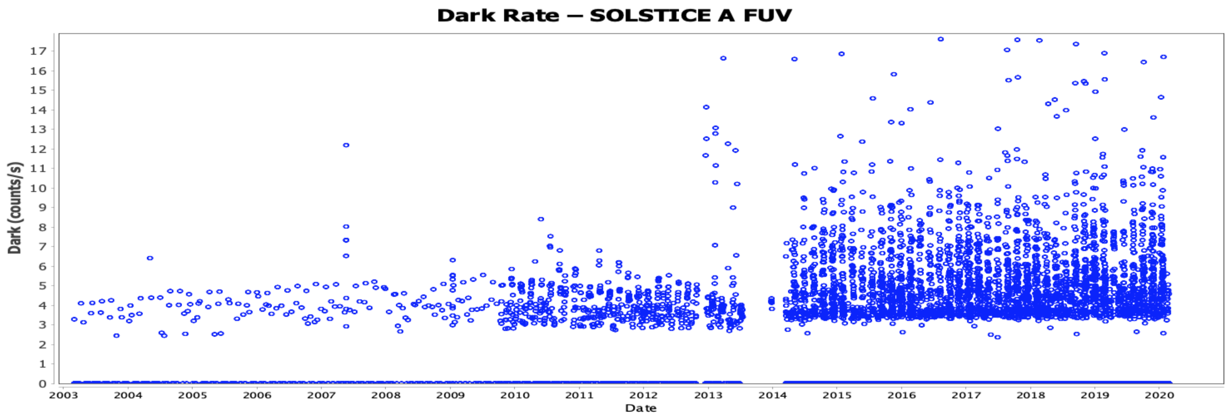
Dark Rate – SOLSTICE A FUV
Dark (counts/s)
Date

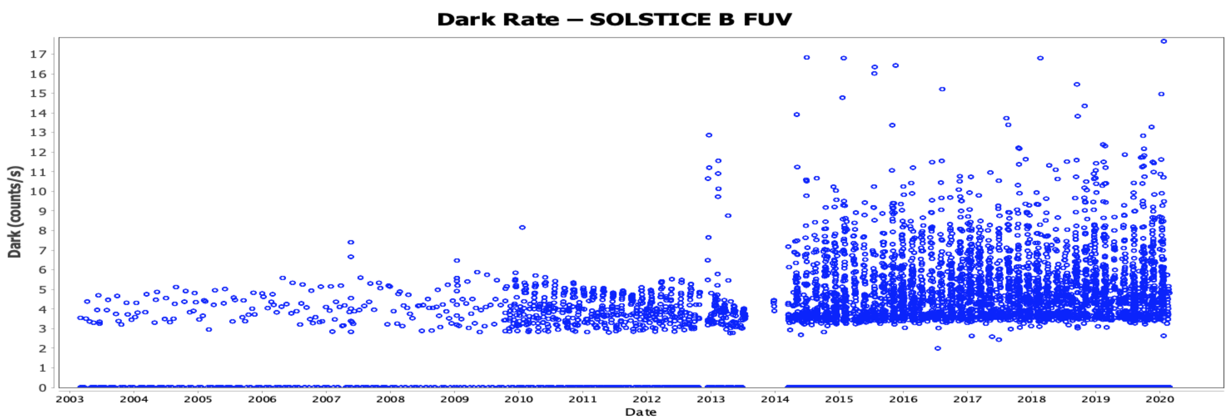
Dark Rate – SOLSTICE B FUV
Dark (counts/s)
Date

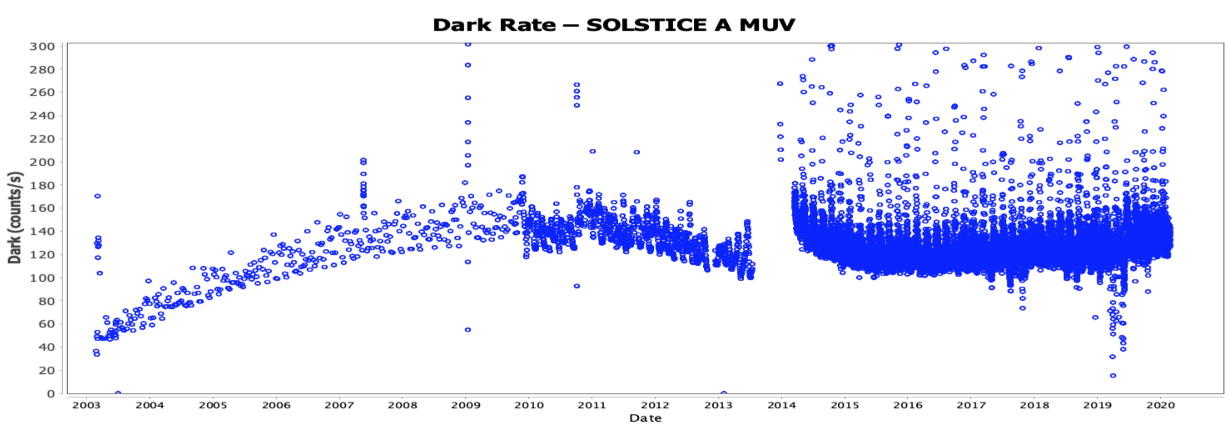
Dark Rate – SOLSTICE A MUV
Dark (counts/s)
Date

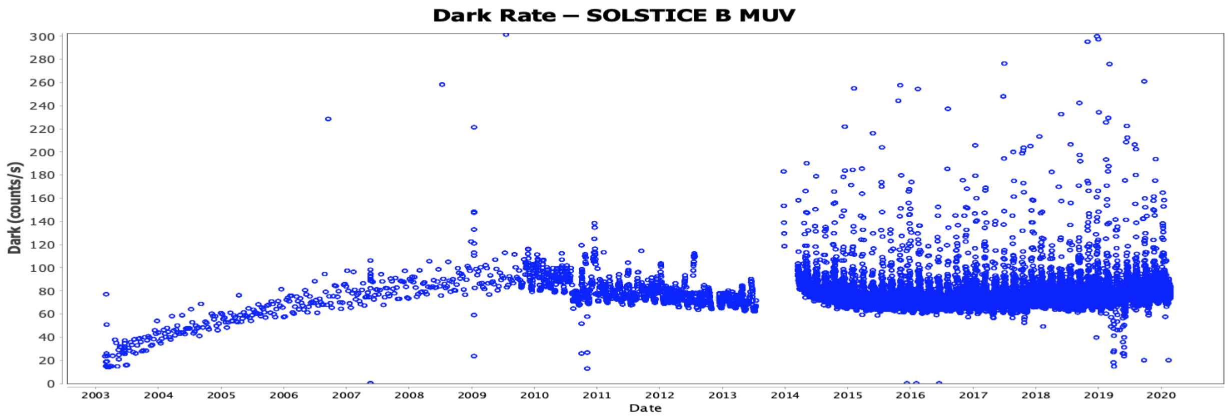

Figure 6. Dark rates for SOLSTICE A and B; FUV and MUV modes. This data was collected during ABComparison experiments throughout the mission.

During the first few years of the mission, dark rates could be estimated by observing dark regions of the sky in stellar mode. After 2006, this was not possible for SOLSTICE A; and after 2010, this became impossible for SOLSTICE B. Figure 7 shows a comparison of the two methods of collecting dark data for SOLSTICE B MUV channel. Both give consistent trends.

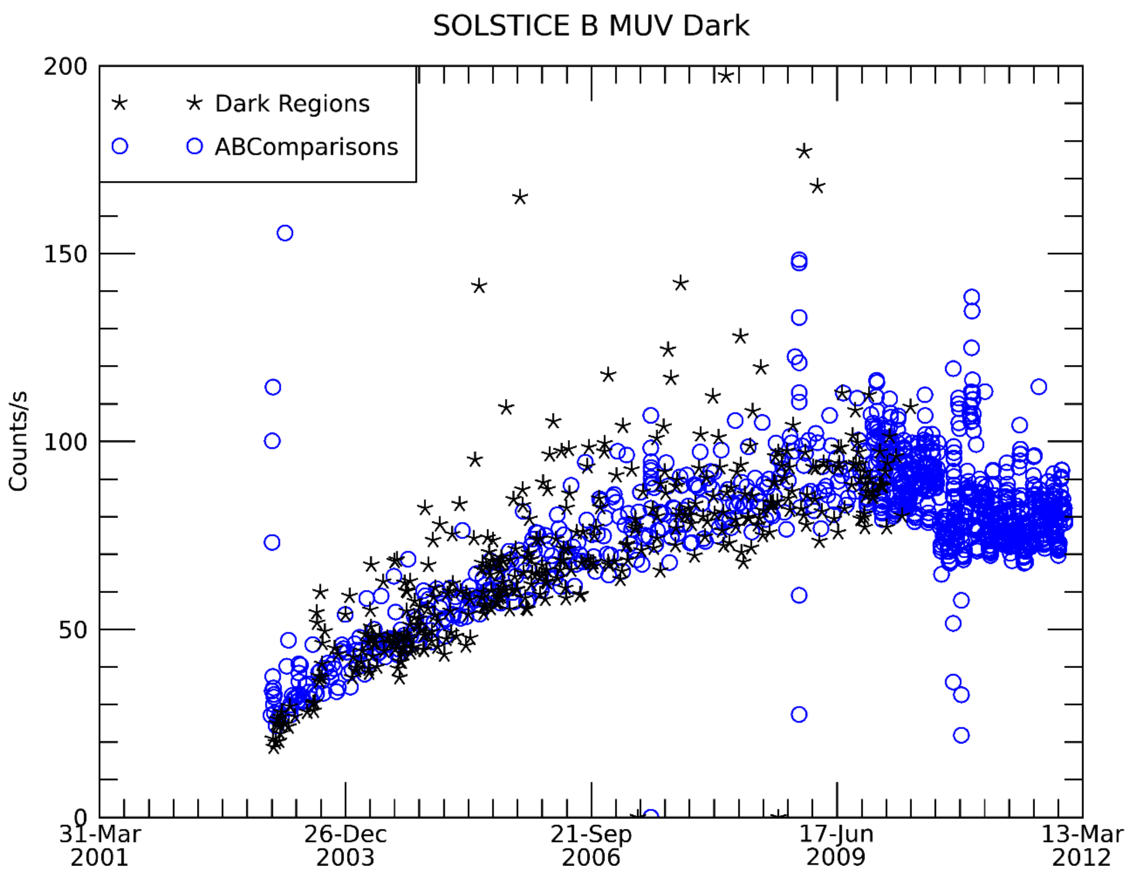

Figure 7. Dark rates for SOLSTICE B MUV determined from eclipse observations of a dark regions and from the inactive channel during ABComparison experiments.

4.3.1.2. Field of View Maps

During the mission prior the first battery anomaly in 2011, the spacecraft would offpoint and dwell on a grid of points during a solar observation to map out the field of view (FOV) near nominal pointing. One of these maps would take many orbits over several days, so the maps were only repeated every six months. Figure 8 shows maps from four epochs at a single wavelength in the MUV. The original ATBD had imagined using these FOV maps to correct for poor spacecraft pointing. The pointing of the SORCE spacecraft was good enough that the magnitude of the pointing correction was too small to be implemented. The uncertainty in the correction is larger than the correction itself. Figure 9 shows the magnitude of the estimated correction due to pointing based on the maps.

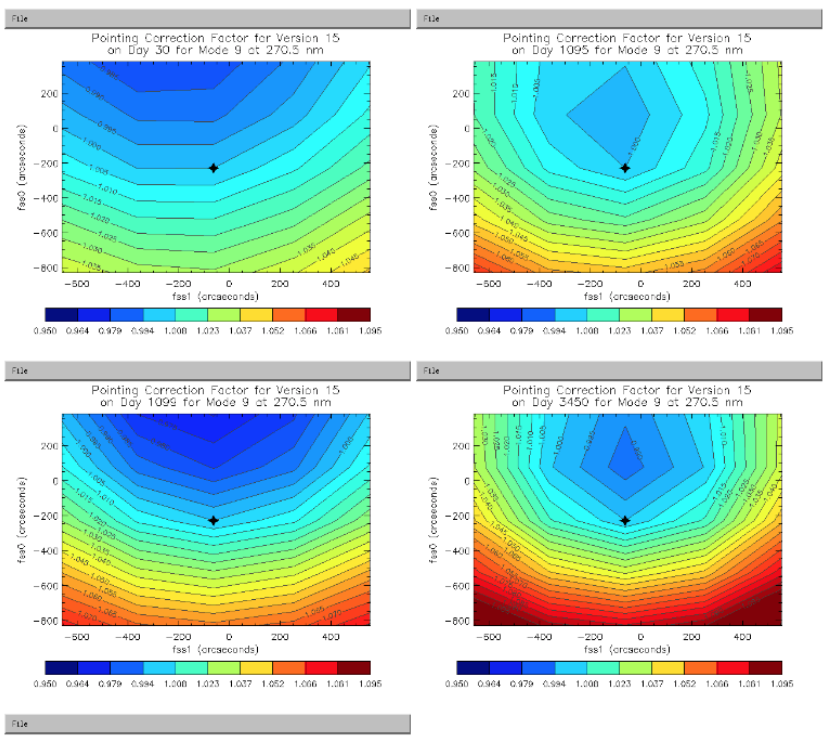

Figure 8. Field of view maps at 270.5 nm throughout the mission. The only significant change was caused by the SOLSTICE A entrance aperture anomaly.

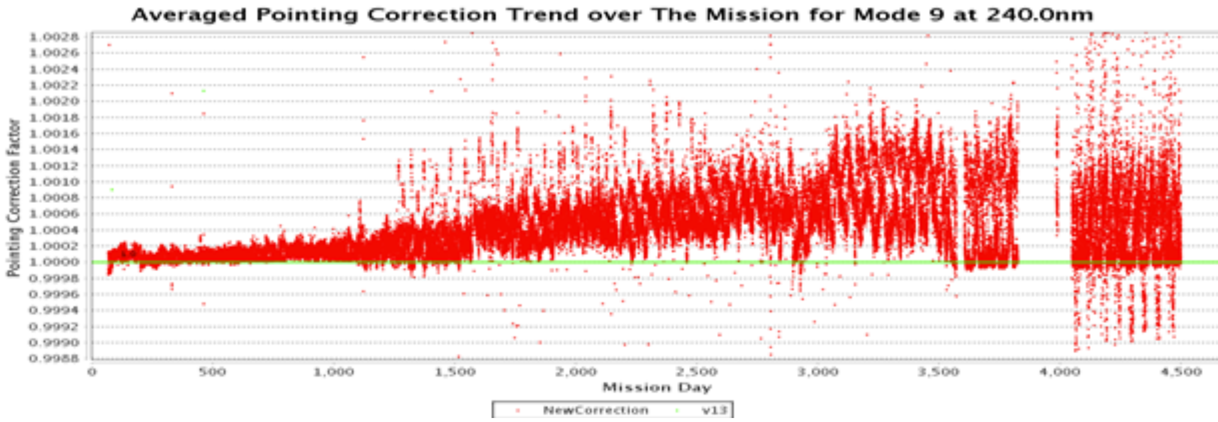

Figure 9. Pointing correction determined from FOV maps. This correction was determined to be small enough that it was not implemented.

4.3.1.3. Cruciform Scans

SOLSTICE made use of the weekly cruciform alignment scans in several ways. First of all, they were used to monitor for shifts in the edges of the field of view. The scans went more than 5 degrees on either side of the nominal boresight, so the locations of the optical baffles were well mapped. The plot of signal as a function of angle has a roughly Gaussian shape and we refer to it as a "haystack." Figure 10 shows an example haystack at a nominal wavelength of 189 nm.

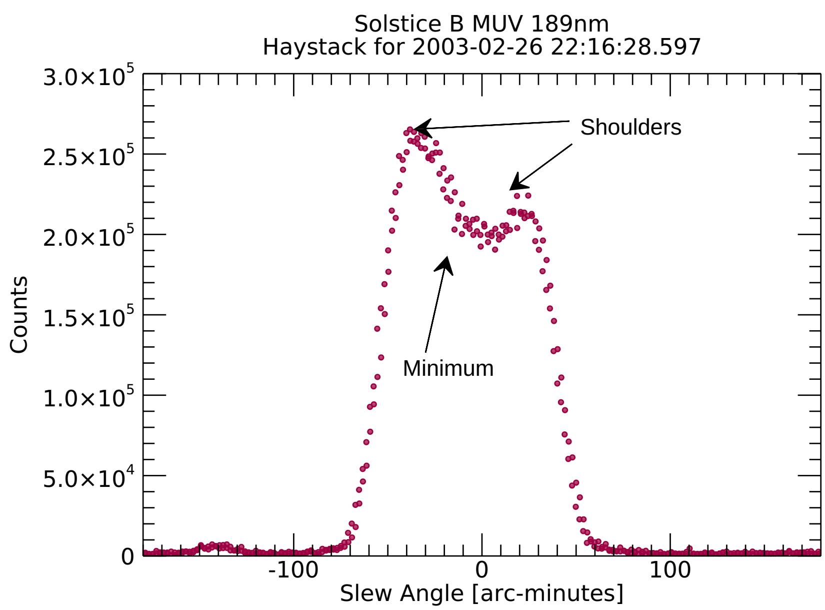

Figure 10. Typical haystack observation during a cruciform maneuver.

The relative shape of the haystack near the center of the field of view tracks the degradation of the portion of the optics exposed to daily solar irradiance relative to the portion of the optics which does not. Non-exposure related degradation factors will affect both regions, so these observations cannot track the total degradation, but they do monitor the "burn in" of the center of the optical path.

SOLSTICE operations during these scans have changed several times over the course of the mission. Originally, the instrument would make a fixed-grating position observation throughout the entire orbit at one of four wavelengths. The four wavelengths would cycle once a week, producing measurements once a month. When it became clear that these observations were capturing the bulk of the degradation, we increased the number of wavelengths from four to eight. The trade-off was that each wavelength was now measured once per eight weeks, but better wavelength sampling was more important. The degradation curves are slowly varying in time, so measurements ever eight weeks was sufficient.

The large scatter for each fixed grating position was due to uncertainty in the measured wavelength. From orbit to orbit, the instrument is power cycled due to the GCI lockups caused by the SAA. When the instrument resets, the instrument tries to find the fiducial on the grating. If it is not found reliably, the offset term in the grating equation changes, thus changing the wavelength corresponding to a fixed wavelength. We solved this problem by commanding the instrument to do a small spectral scan throughout the spacecraft maneuver. The Sun's spectrum is very rich, so a 25-step mini-scan captures enough spectral features to correct the wavelength scale throughout the maneuver.

The feature near -150 arc minutes is persistent, and its cause is unknown. It is well beyond the field of view during normal operations and its magnitude is small. The SOLSTICE team has examined several possible causes, but none have been definitively confirmed.

Figure 11 shows a time series of the ratio of the center of the field of view to the shoulder for one of the four wavelengths. The data has been fit with a linear function of time. The reduction in residuals in 2007 is due to the change to a mini-scan instead of a fixed wavelength. This type of calibration observation stopped in 2012 after spacecraft operations went to RTS mode.

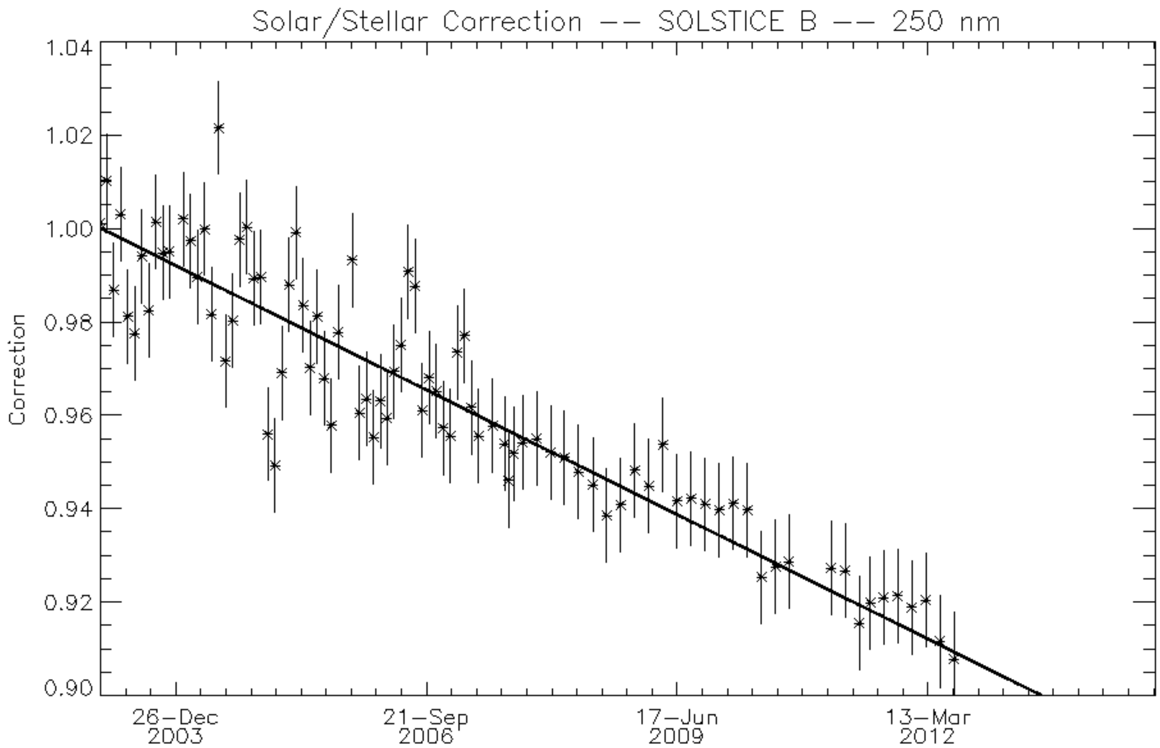

Figure 11. Relative change of the solar-exposed optics to the edge. Scatter decreased after changing to a mini-scan during the spacecraft maneuver.

Tracking the change in responsivity of the center of the field of view at the four added wavelengths has been a challenge. There were no preflight measurements to normalize to. Extrapolating back to the beginning of the mission added additional uncertainty. The uncertainty in the extrapolation was minimized by using a linear function of time rather than a polynomial or exponential. Interpolating in wavelength guided our analysis, but as will be shown later, this introduced significant systematic error which was not corrected until version 17. Figure 12 shows the observations from one of the four additional wavelengths extrapolated back to the beginning of the mission.

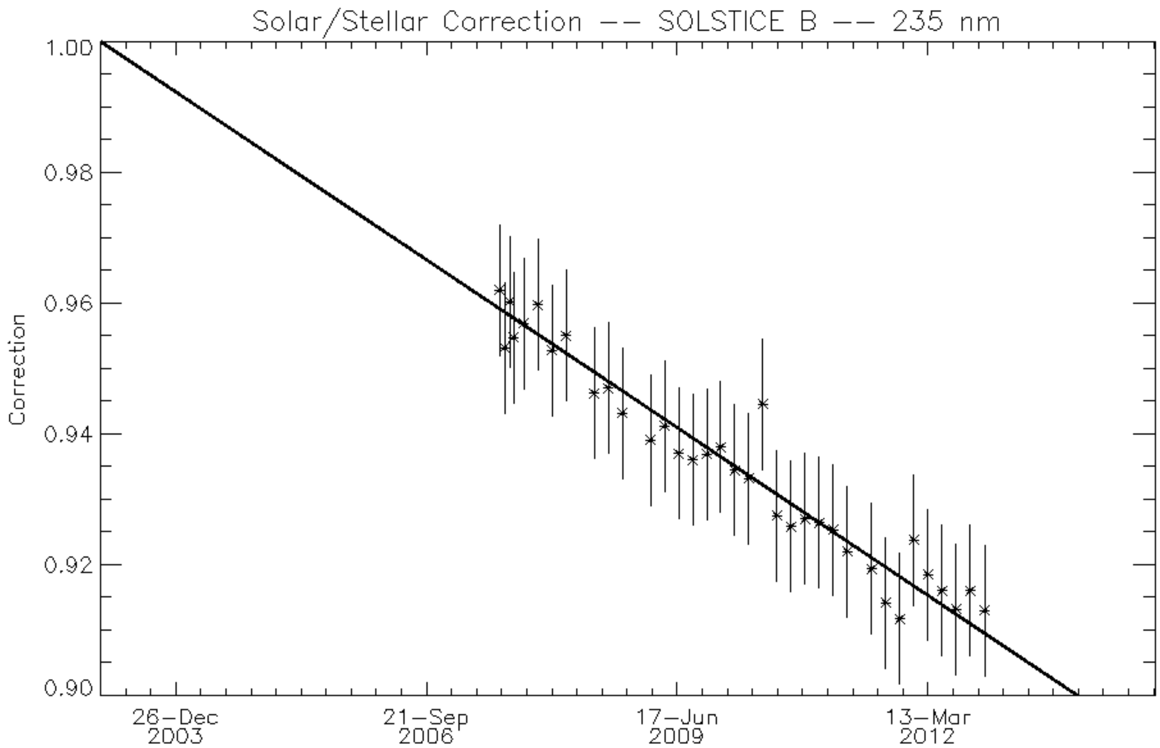

Figure 12. Relative change of signal for one of the four wavelengths that was added in 2007.

In DO-Op mode, the cruciform maneuver was replaced by an offset to 22.5 arc minutes off normal pointing, with a full spectral scan at this one position. Commanding a spacecraft slew was not possible in DO-Op mode, so a compromise was made in order to continue to make field of view correction calibration observations. The ratio of the center of the field of view to the offpoint produced one unexpected result. There was more variation with wavelength than had been captured by the earlier measurements. Interpolating between the eight wavelengths sampled by the cruciforms had missed important structure. Figure 13 (green curve) shows the eight sampled wavelengths with linear interpolation between them. The blue curve shows the ratio determined from the DO-Op offpoint observations.

Section 4.4 will describe how these cruciform and offpoint observations are used to correct the instrument degradation.

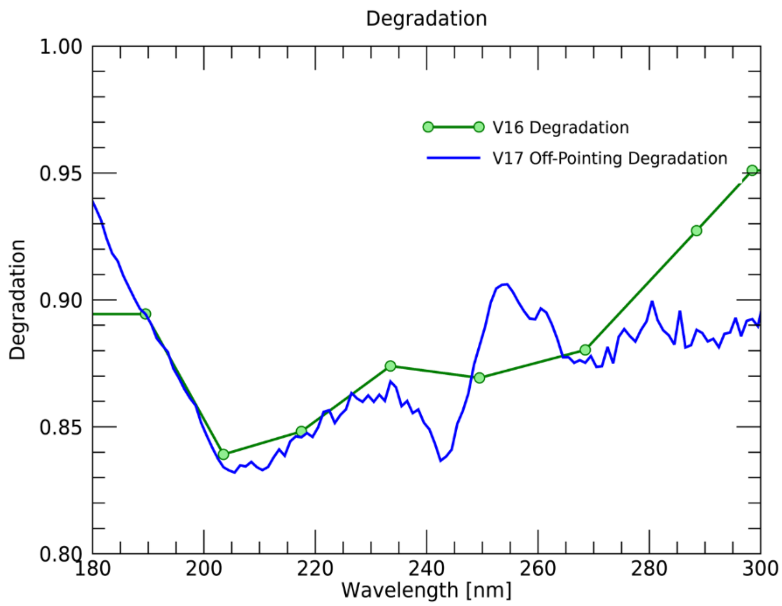

Figure 13. Ratio of center field of view to the edge for the primary mission cruciforms and the DO-Op mode offpoint.

4.3.1.4. Filter Transmission and Dead Time

There are two neutral density filters in the MUV optical path. The filters are on bi-stable mechanisms and can each be independently removed from the light path. The purpose of these filters is to reduce the signal on the detector for wavelengths that would otherwise cause the photomultiplier tube to saturate (i.e. become nonlinear). A standard calibration observation is to cycle through the four possible filter configurations: no filter (00), filter 1 only (10), filter two only (01), and both filters (11). At each filter configuration, the instrument would scan the MUV spectrum.

During this filter transmission observation, it is necessary to compare to observations with higher count rates than desired at some wavelengths. Therefore the filter transmission and dead time cannot be determined independently. Figure 14 shows the filter transmission for a range of assumed dead times. The linear fit that reduces the variance the most is determined to be the dead time for data processing.

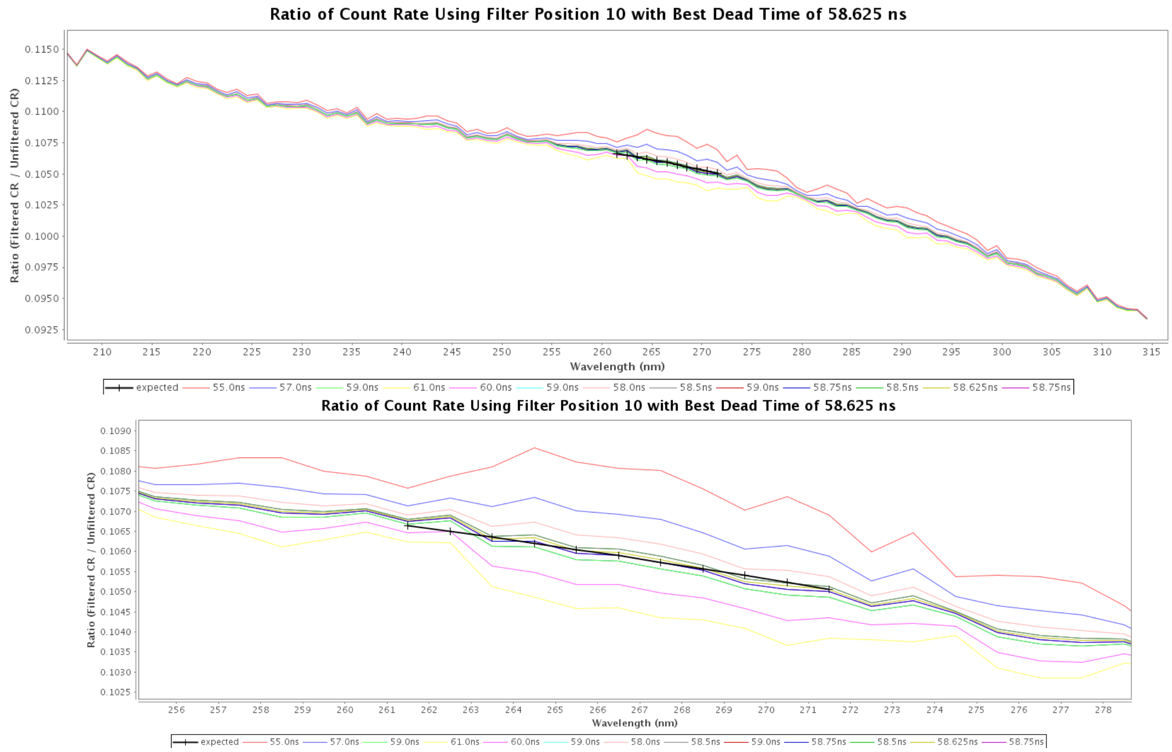

Figure 14. The top panel shows the filter transmission for a range of dead times. The lower panel is a zoomed in part of the plot showing the region with the highest count rates.

Filter transmission measurements were taken throughout the primary mission, and the calculated dead time slowly changed as shown in Figure 15. After the long safe hold, the dead time determined by this method is a lower value than before the vacation. Surprisingly, it has also remained constant until the end of the mission. There is no SOLSTICE calibration observation that can definitively determine a physical cause for this behavior. The empirically measured value is our only estimate.

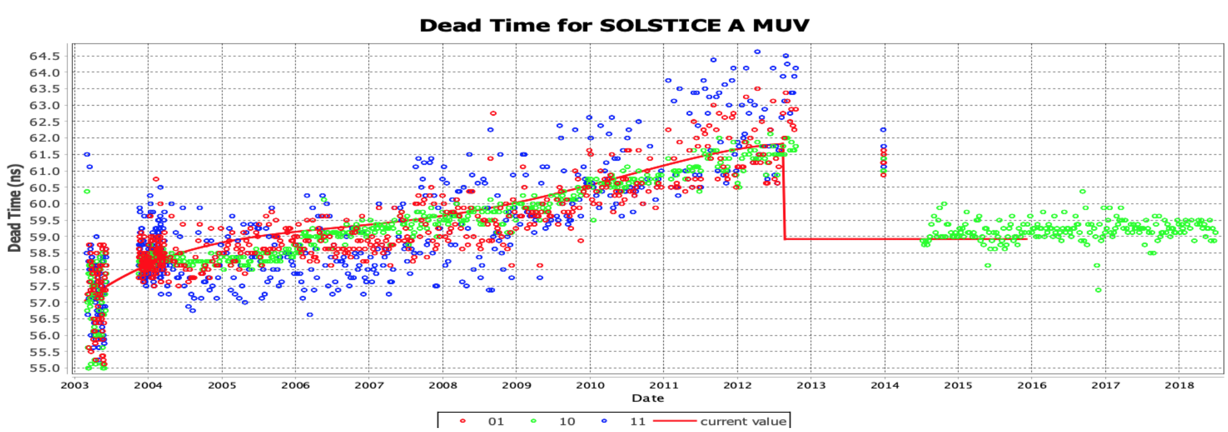

Figure 15. Dead time determined from filter transmission experiments.

4.3.2. Algorithm Changes

4.3.2.1. Wavelength Scale

The determination of the wavelength scale in the original ATBD for each spectral scan is a least squares fit to a reference spectrum. For the first few years of the mission, this involved non-physical shifting and stretching the spectrum. Analysis of in-flight data showed that the spectrum did not stretch. The SOLSTICE grating drive was very linear. We modified the algorithm to use the grating equation and fit one parameter, the grating offset, to find the least-squares match to the reference spectrum. This works better than the original algorithm for most cases. It is insufficient for observations that span a significant portion of an orbit. At UV wavelengths, the Doppler shift from the orbital motion introduces a shift of more than a third of a (27DN) grating step. The Mg II mini-scan experiment uses smaller steps (9DN), so the correction for spacecraft motion is essential. Figure 16 shows the Doppler correction factor for a typical orbit. We make use of the SORCE TIM processing system to determine this factor for each orbit. Figure 17 shows the size of the correction in grating steps as a function of Doppler factor.

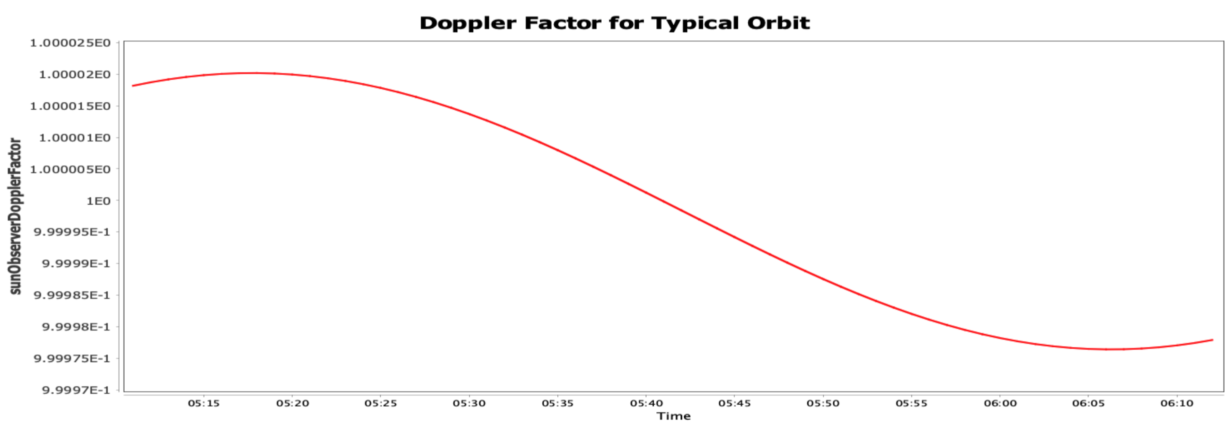

Figure 16. Doppler factor for a typical orbit.

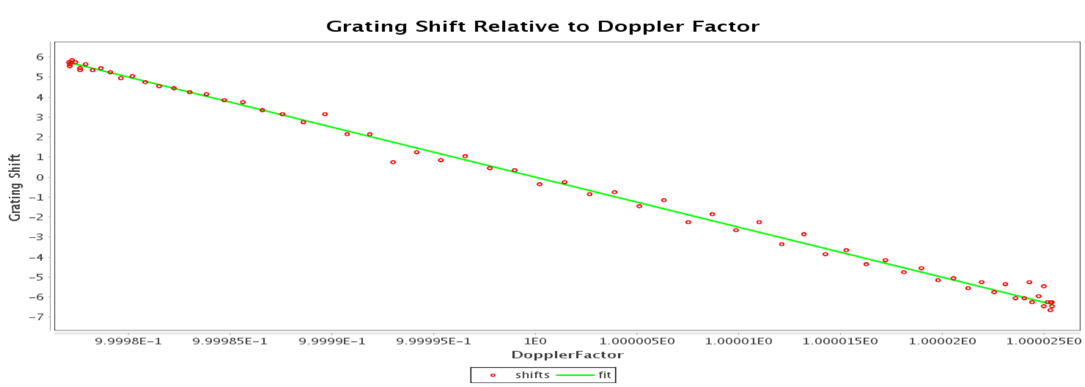

Figure 17. Magnitude of the shift in grating position from Doppler factor at 280 nm.

As an example of the effect of this wavelength correction, Figure 18 shows the wavelength samples using only a single shift for the entire orbit (red X's). Application of the Doppler correction produces the blue dots. The spectral feature is clearly sampled more accurately after the correction.

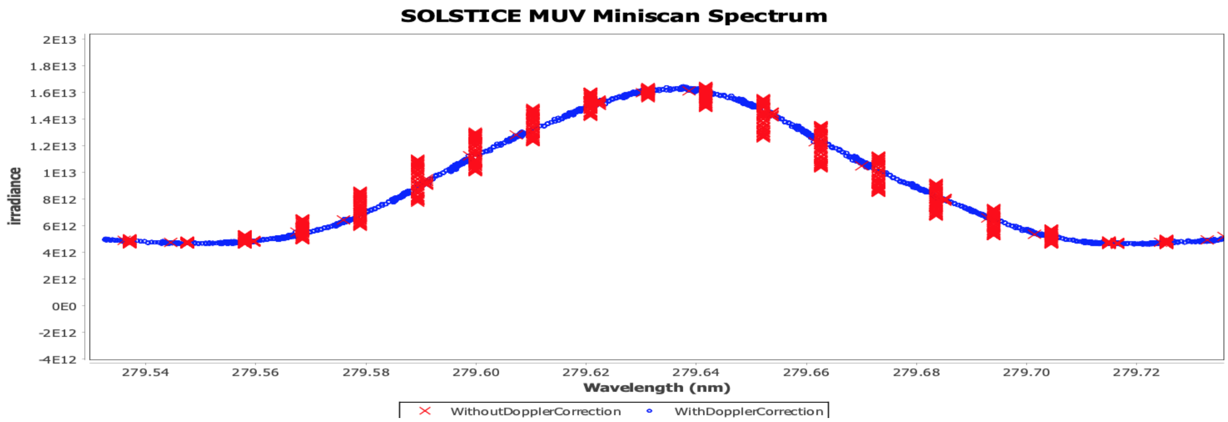

Figure 18. Small section of the spectrum taken during a full-orbit mini-scan activity. The red X's show the wavelengths indicated by the shift-only algorithm. The blue dots are the samples after adjustment for Doppler shift.

4.3.2.2. South Atlantic Anomaly

In the original ATBD, the region that defined the SAA was a fixed polygon in latitude and longitude. The map had been developed in the late 1980s for the UARS mission. Observations from SORCE confirmed ground-based magnetometer data that shows the SAA slowly moving westward. Rather than updating a map polygon periodically, we now use SOLSTICE itself to determine if data is corrupted by elevated background counts. On each SOLSTICE, there are two detectors. While one is taking solar data (active channel), the other (inactive) channel is measuring the background. We have set a threshold as shown in Figure 19. In this figure, the blue data is from the FUV channel while in MUV mode. The green curve is a fit to the background FUV detector's data. The red curves are scaled versions of the MUV solar count rate spectrum. The threshold is met if the estimated background in the active channel exceeds 1% of the signal. In the example shown here, anywhere that the green curve is greater than the red curve, the data is corrupted by the SAA.

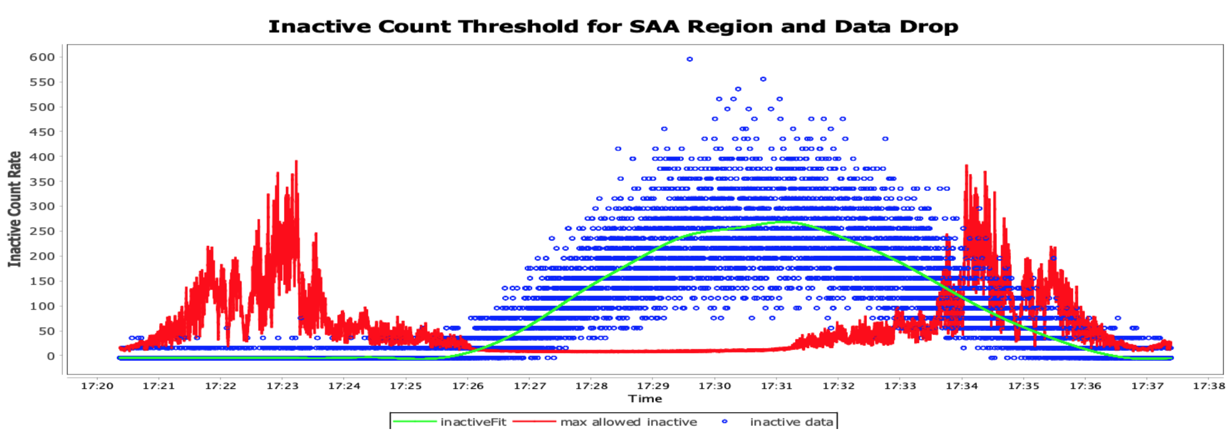

Figure 19. Threshold for count rate on the inactive channel to set the SAA flag.

4.3.2.3. Correction to 1 Astronomical Unit

The main correction to a standard 1 AU distance from the Sun is a simple 1/r-squared calculation from the ephemeris. That correction is large (nearly 9%) and is easily removed from the data. Figure 20 shows the v14 SOLSTICE level 3 data in blue. There is a clear 1-year period in the data. We have determined that this is due to the fact that the angular size of the Sun changes throughout the year. Figure 21 shows a typical haystack as a function of slew angle. When the Sun's angular size is small, it occupies only the more burned-in part of the optics. When it appears larger, the average responsivity is higher because some of the less burned-in part of the optics is exposed. This "second order" 1-au effect can be corrected by using the haystack shape as a function of time. The red curve in Figure 20 is the v15 data after the correction.

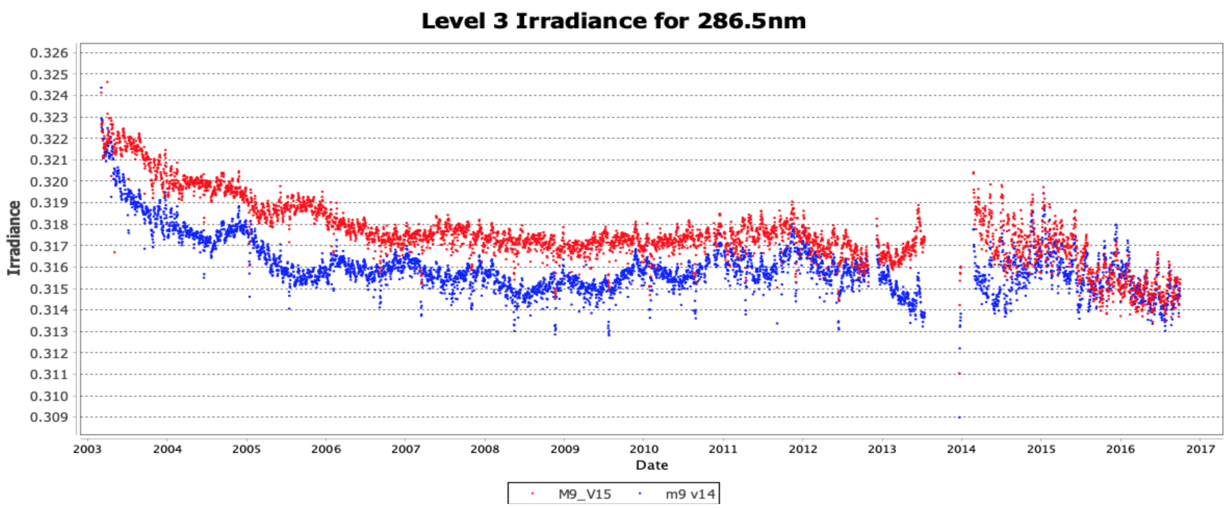

Figure 20. Version 14 SOLSTICE data in blue shows a clear annual signal. The red data is version 15 after the application of the second order 1-au correction.

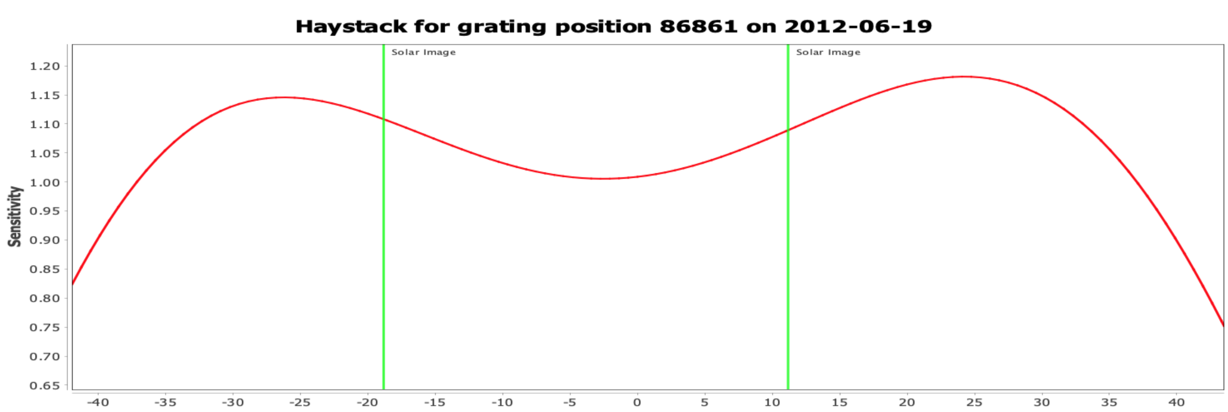

Figure 21. Typical haystack shape. The two green lines denote the size of the Sun on that date. When the Sun is closer, the size increases, raising the average responsivity.

4.3.2.4. Change to Calculation of Corrected Counts

The equation for converting measured signal, S, to a corrected count rate was given in McClintock et al. (2005b) as:

$$C(\lambda,\ \tau,\ Dc,\ Sl,\ St) = \frac{S(\lambda)N(\tau) - Dc - Sl(\lambda) - St}{\Delta t} \qquad (3)$$

Where N is the nonlinearity factor, τ is the detector dead time, λ is wavelength, and Δt is the integration time. Dc, Sl, and St are the dark current, scattered light, and stray light respectively. There are several updates to this equation in the current data processing system.

$$C(\lambda,\ \tau,\ Dc,\ Sl,\ St) = \frac{(S(\lambda)N(\tau) - Dc - Sl(\lambda) * T\_f) * Gain}{\Delta t * T\_f * f\_pointing} \qquad (4)$$

The temperature gain (Section 4.3.2.5) was inadvertently omitted. It was also determined that stray and scattered light would need to pass through the filter to reach the detector, so those signals would be attenuated by the filter transmission. It was also determined that there was no advantage to treating stray and scattered light separately, so they have been combined into a single term. The pointing correction (Section 4.3.1.2) has been moved to this part of the measurement equation in the processing system.

The stray and scattered light level was determined during an inadvertently large grating offset. A spectral scan was done well outside the wavelength range where the MUV detector has responsivity (Figure 22). This additional background is taken to represent the stray and scattered light. Since the configuration of SOLSTICE A and SOLSTICE B are nearly identical, this level is also used as the background of SOLSTICE B.

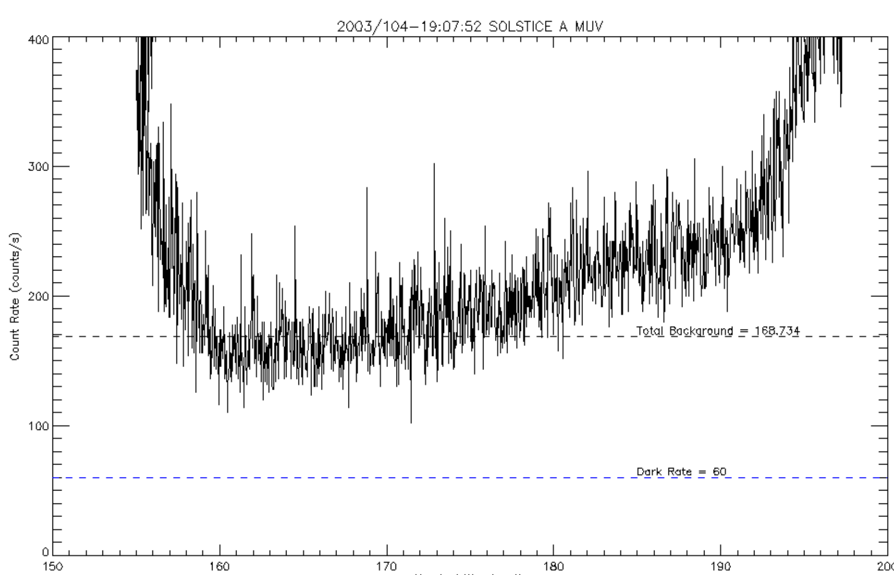

Figure 22. Spectral scan taken beyond the range of SOLSTICE A's MUV responsivity. After correcting for dark rate, the remaining background level is shown.

4.3.2.5. Temperature Gain

The change in responsivity as a function of wavelength was measured during the ground calibration; however, the in-flight behavior of the detector was not the same as it was on the ground. In general, the temperature control of the instrument has been good, but there has been a systematic decrease of the temperature over the mission. The decrease has been due to operational changes to the spacecraft to accommodate the decreasing battery capacity. Figure 23 shows the data from the PMT rear thermistor averaged over each orbit.

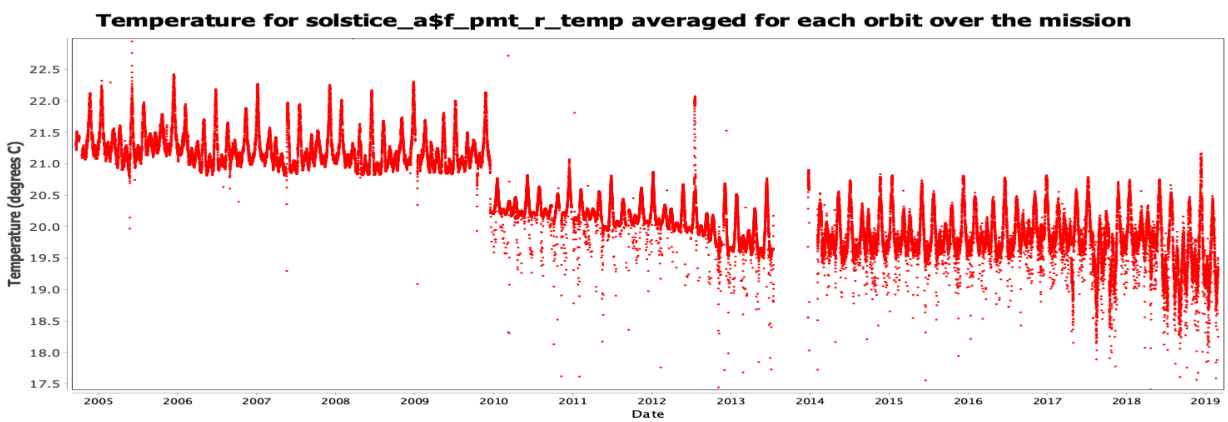

Figure 23. Orbit average of the temperature of the rear of the PMT.

We have made use of time periods where the instrument warms up rapidly. We have chosen a reference temperature of 20C, and then analyzed data where the instrument temperature changes over a day or a few days. At many wavelengths, the SSI does not change appreciably over that time span, so changes in the SOLSTICE signal are due to temperature changes. Using many such time intervals, there will be no systematic correlation to solar activity. Figure 24 shows the change in measured signal as a function of temperature for many time ranges. The ratio relative to 20C is taken to be the temperature gain of the instrument. It is assumed that over this temperature range, a linear fit to the data is appropriate.

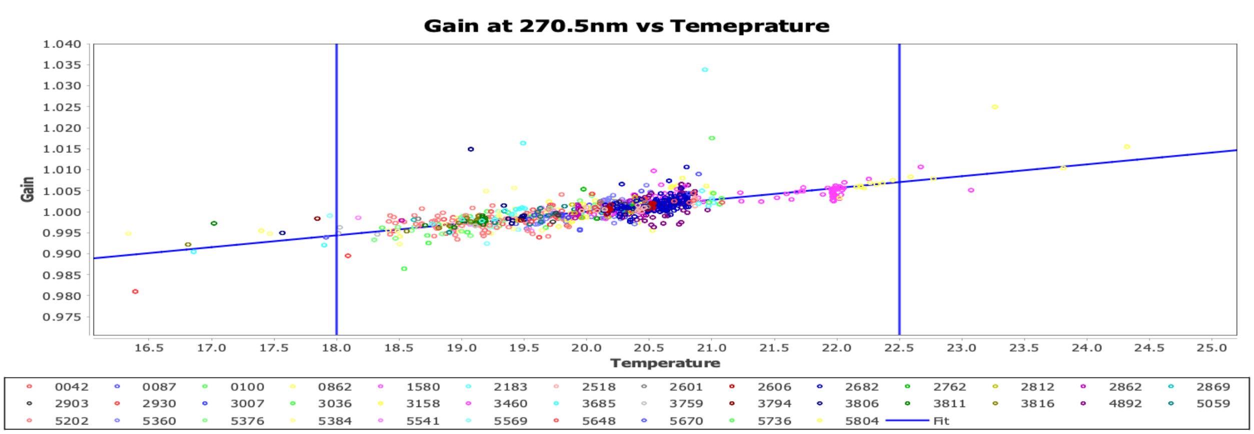

Figure 24. Variation with temperature of the spectrum near 270.5 nm. The different colors are

from different time periods, shown in Mission Day. This data includes data from mission day 42 to 5804.

Since the temperature has a systematic decrease throughout the mission, this temperature gain causes a long-term decrease in the Level 3 SSI data product. Figure 25 shows the magnitude of the temperature correction on the final Level 3 data product. It shows the ratio of a six-month average at solar minimum in 2008 compared to a similar six-month average in 2019. The red curve is the V17 data product without the correction, blue shows the ratio with the correction applied. The difference in irradiance is about 1% over 11 years. This is a significant fraction of the solar cycle amplitude at many of these wavelengths.

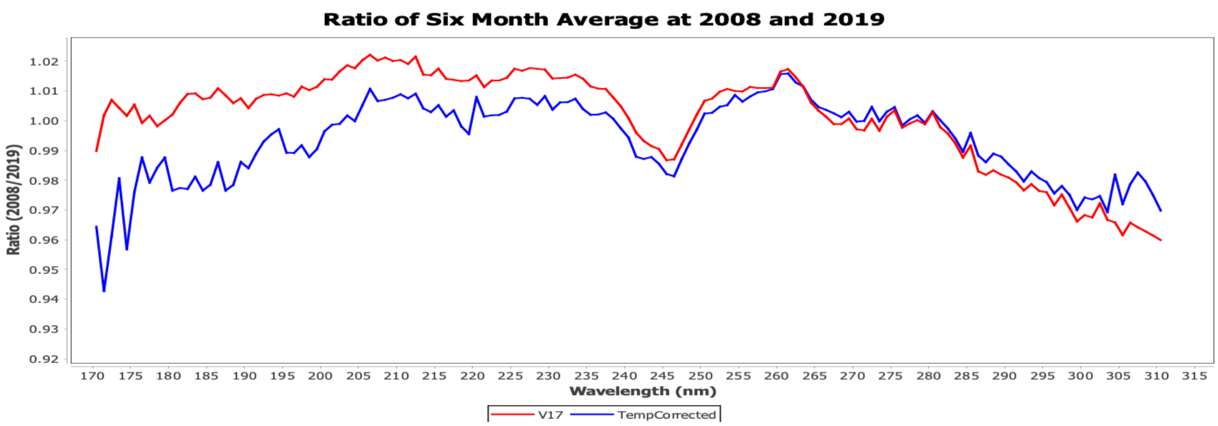

Figure 25. Magnitude of the change in SSI from one solar minimum to another due to the temperature correction alone. This plot shows the ratio of irradiances in 2008 to 2019 with and without the temperature correction.

4.4. Degradation

The SOLSTICE degradation function is determined by two sets of calibration measurements. The first set is observations of bright early-type stars. The second set is the cruciform alignments and DO-Op mode offpoints. The stellar observations use a large portion of the optics, primarily the part that is rarely exposed to sunlight. The ratio of sun/star exposure area on the first mirror (M1) is 10-to-1. It is 3-to-1 on the second optic, the grating. What the stellar observations do capture is any degradation of the detector and/or electronics. These components can be damaged by exposure and also by the harsh space environment.

The primary measurement of SOLSTICE is SSI. In order to accurately estimate the degradation of the solar signal, we also need to fold in the “burn in” of the portion of the optics exposed to the Sun. Comparing the center of the field of view to the edges as described in Section 4.3.1.3, we can estimate the portion of the degradation function that is not well measured by the stellar observations. Snow et al. (2005a) describes the degradation technique for the primary mission.

4.4.1. Stellar Observations

During the primary mission, bright early-type stars were observed on a regular basis. These stellar irradiances were fit with a least-squares technique that normalized each star’s absolute magnitude and fit an exponential function. An example fit is shown in Figure 26. The upper left plot of Figure 26 shows a time series of the uncorrected stellar irradiances at one fixed wavelength. The lower left plot shows the irradiances after normalization along with the exponential fit. The dashed lines show the 1-sigma uncertainty in the fit. The upper right panel shows the histogram of corrected irradiances to check if the mean is unity and if the samples are normally distributed (i.e. the reduced chi-squared is of order unity). The lower right shows a legend of which stars are used, along with their average count rate.

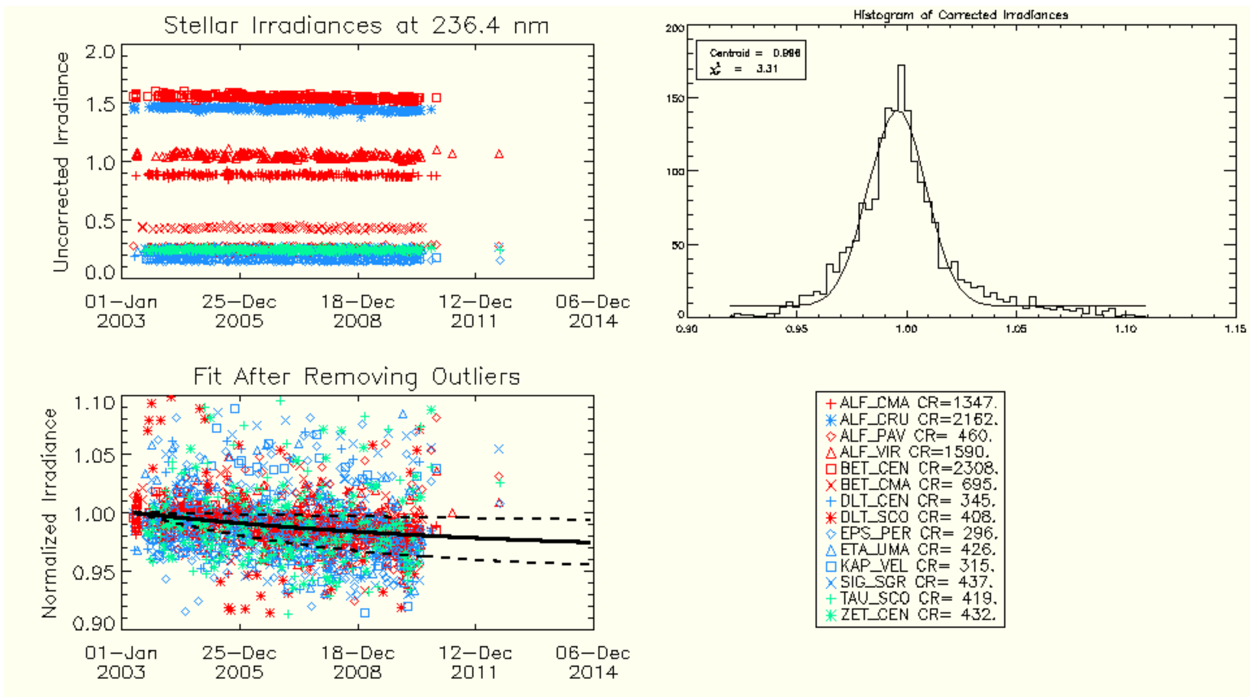

Figure 26. Stellar degradation correction. See text for descriptions of each panel.

Figure 27 shows the degradation as a function of wavelength for the two channels of SOLSTICE B. As mentioned in Section 4.2.2, no stellar measurements were taken with SOLSTICE A after January 2006. All degradation corrections are determined from SOLSTICE B. The uncertainty in the exponential fits is zero at the beginning of the mission by definition, and grows at about 0.2% per year. The exact amount depends on wavelength, but all are similar.

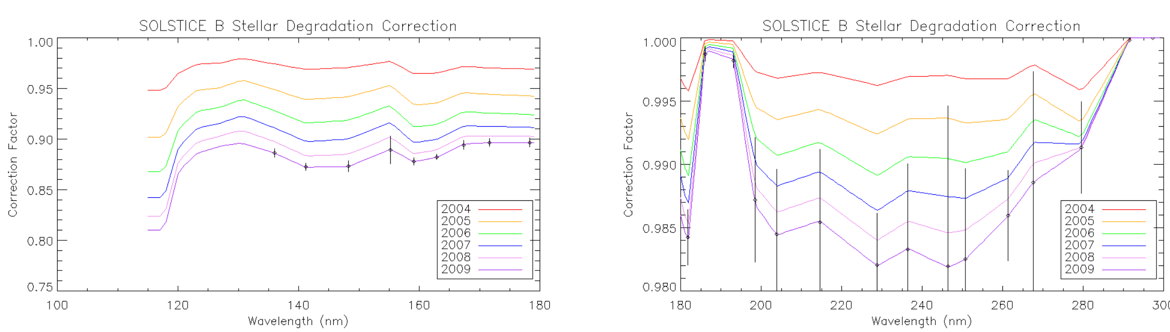

Figure 27. Stellar degradation summary for SOLSTICE B FUV and MUV. One curve per year is shown, and the error bars are shown only on the last curve for clarity.

After the primary mission, degradation of the spacecraft battery made routine stellar measurements impossible. During the DO-Op phase of the mission, a handful of stellar observations were obtained. Instead of fixed wavelengths, these observations were FUV spectral scans. The spectrum allowed us to gather information at many wavelengths in a short amount of time, but at lower signal to noise ratio. These observations were made during the solar period of the orbit, since the instrument and most spacecraft systems are powered off during eclipse. To make this measurement, the target needed to be within an annulus 20 to 30 degrees away from the Sun. This range was chosen to ensure that the instruments were free from any solar glint, yet not far enough to reduce the power to the solar panels (cos(30°) =.86) below an acceptable level. An additional observing constraint was that there needed to be ground station available at the end of the solar period to downlink the data. These constraints led to only a handful of successful stellar observations during DO-Op mode. But the number of successful observations was greater than zero!

Figure 28 shows the data for alpha Virgo from the fixed-wavelength observations of the primary mission (red dots) and the stellar spectral scans from both the primary and DO-Op. The purple curve was determined from only the fixed-wavelength observations. The correction using the DO-Op observations is still a research project for version 18. These preliminary results show that extrapolating the fit from the primary mission was reasonable for this wavelength.

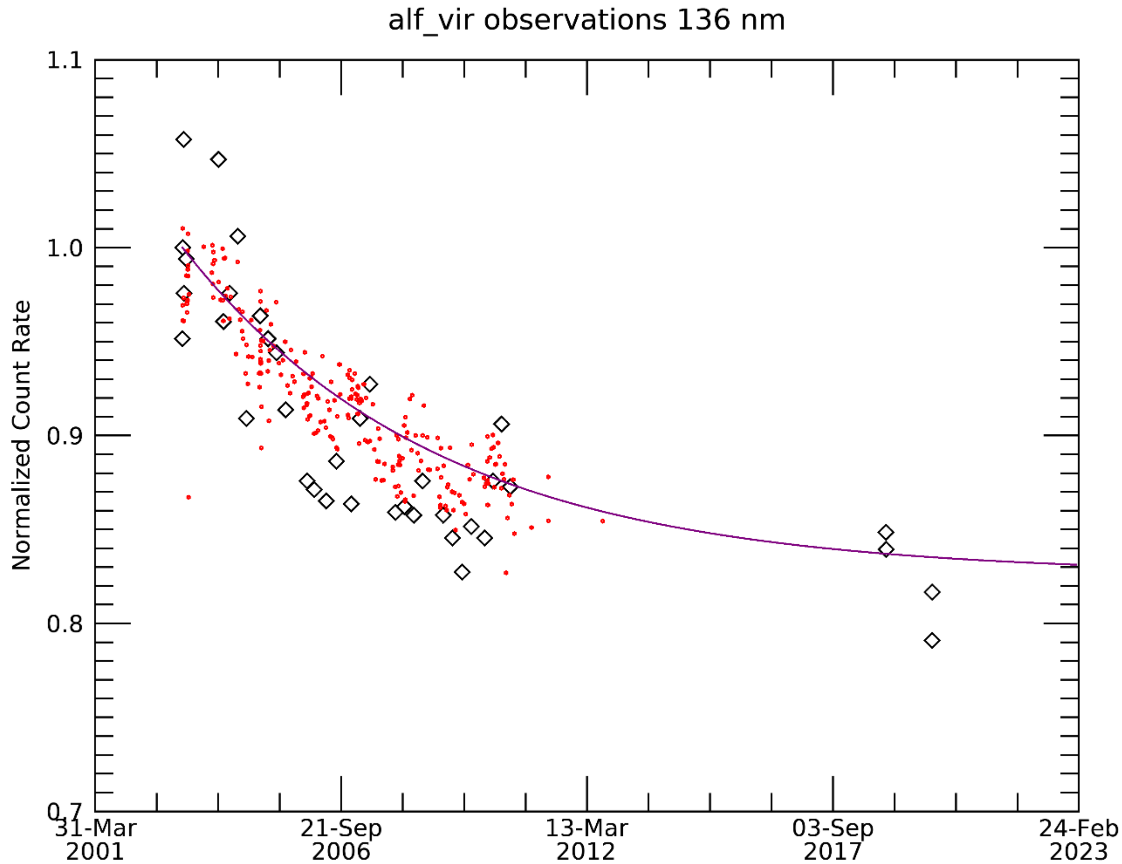

Figure 28. Observations of alpha Virgo at 136 nm with SOLSTICE B. Red dots are fixed-wavelength observations, the purple curve is the exponential fit to that data, extrapolated to the end of the mission. The diamonds show the observations at this wavelength from spectral scans, both during the primary mission and during DO-Op mode.

During the DO-Op era, the two instruments alternate between FUV and MUV modes each solar period. This has resulted in greater solar exposure per day for the SOLSTICE B MUV channel. Previously, it had only been used during ABComparison experiments (weekly for the first five years, then one orbit per day until DO-Op). The amount of solar exposure on the optics is basically unchanged since SOLSTICE has no shutter and the optical path for the two modes is the same up to the ellipse (see Figure 1 of McClintock et al. 2005a).

The MUV stellar observations were all collected prior to DO-Op mode. In our instrument model, degradation of the detector and electronics is all captured in the stellar degradation term. The exposure per day in that time period was lower than in DO-Op, so we have applied a correction for exposure time to the MUV stellar exponential function. Figure 29 shows the counts per day and the cumulative exposure as a function of time for SOLSTICE B MUV. The cumulative counts per day is roughly linear during the two epochs, so the slope of the DO-Op portion is used to create an exposure time correction for the MUV stellar degradation function.

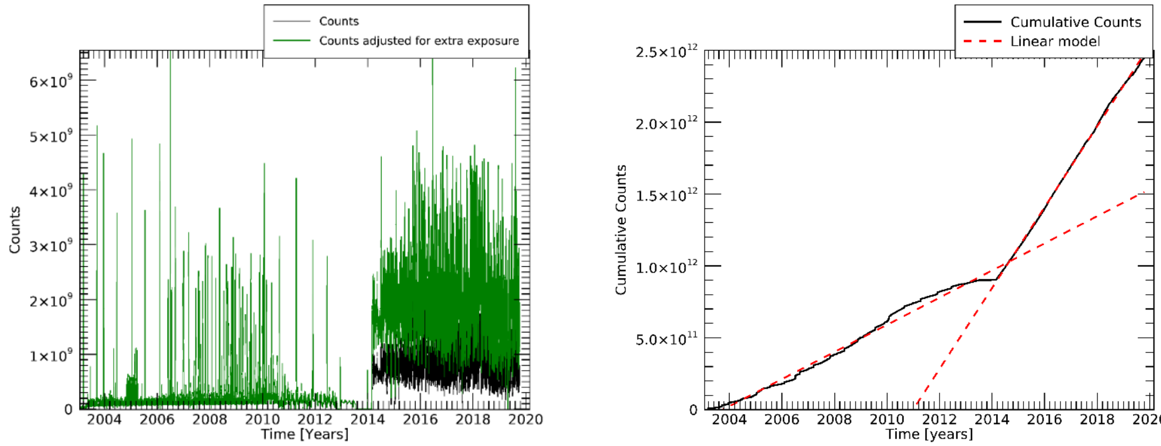

Figure 29. (left) Counts per day over the mission for SOLSTICE B MUV. (right) Cumulative counts over the mission. The two linear fits are used to determine the correction to exposure time.

4.4.2. Solar/Stellar Field of View Correction

The other component of the degradation analysis is the cruciform and offpoint observations that measure the difference in field of view between the solar mode and stellar mode. As was described above, the cruciforms were used to measure the FOV difference at four wavelengths at the beginning of the mission, and then expanded to include four additional wavelengths later. In DO-Op mode, a full MUV spectrum is collected at an offpoint position. The trend inferred from the cruciform analysis prior to version 17 was not consistent with the trends of the offpoint data. Figure 30 shows the time series for one wavelength. The red data points show the haystack analysis with an estimated normalization factor. The red curve was the trend from version 16 inferred from that data. The offpoint data (blue) clearly have a different trend.

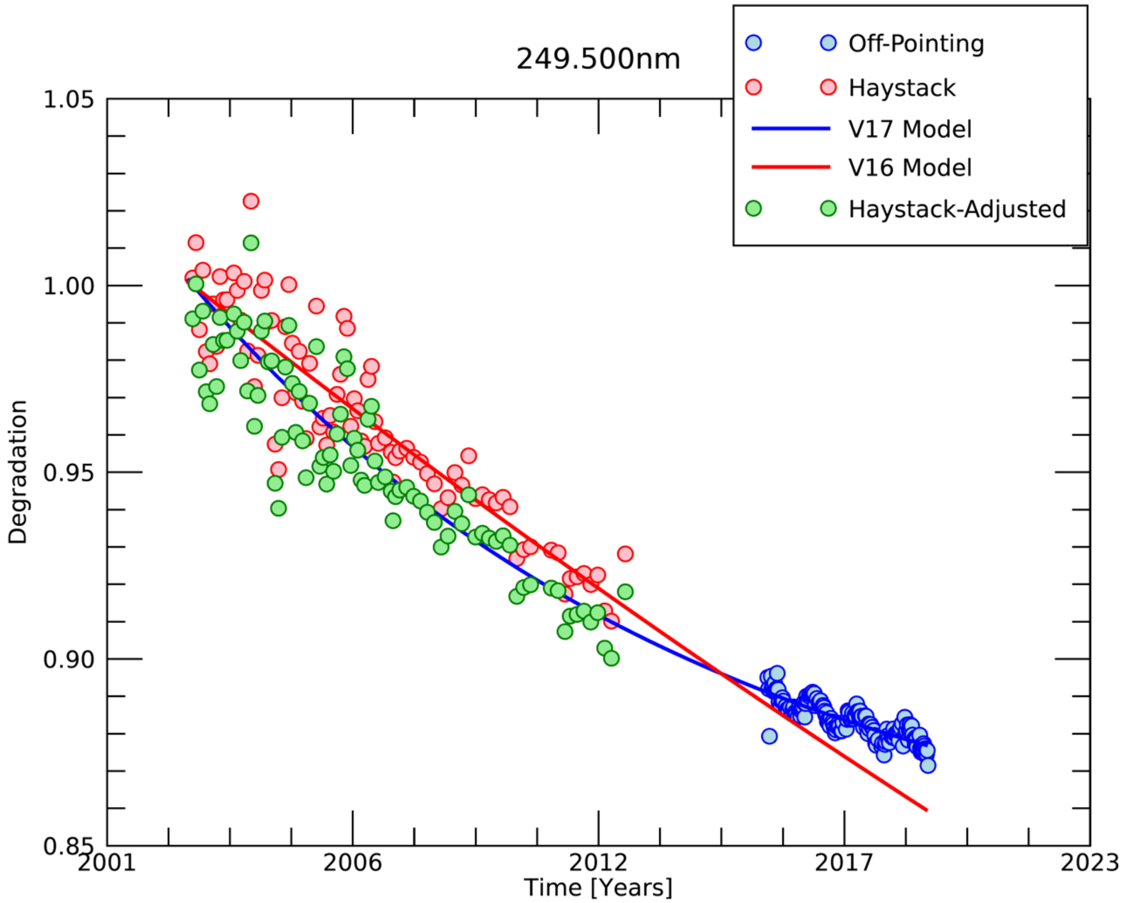

Figure 30. Solar/stellar field of view measurements for one wavelength.

The solution was to do a least-squares fit to the DO-Op offpoint data and the haystack data, with the normalization of the haystack data as one of the fit parameters. There was no preflight data to constrain that normalization. The blue curve in Figure 30 shows the new estimate of the degradation function for the full mission. The shape of the ratio as a function of wavelength shown in Figure 30 was used to interpolate between haystack observations going back to the beginning of the mission. The degradation correction at t=0 is assumed to be 1.0 everywhere, and then smoothly gains the offpoint shape. Figure 31 shows a surface plot of the solar/stellar correction as a function of time and wavelength, along with the data that was used to fit the surface.

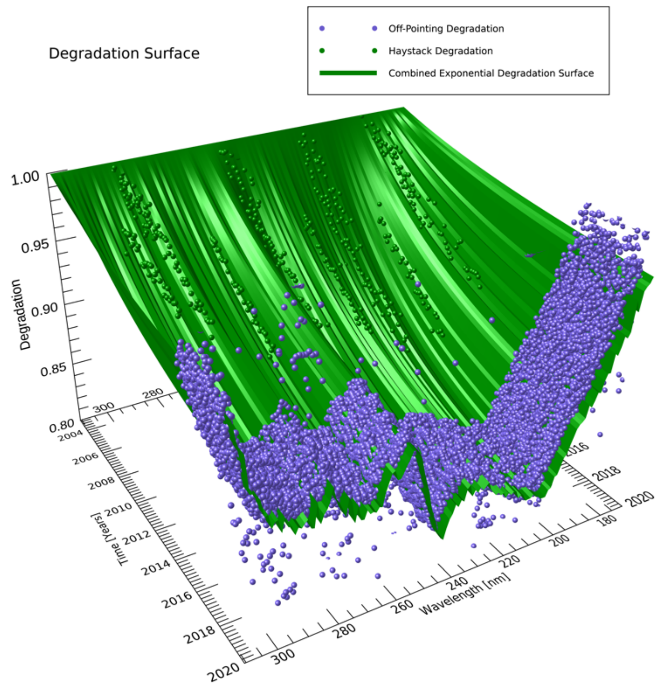

Figure 31. surface plot of solar/stellar correction as a function of wavelength and time.

This correction has currently only been implemented for the MUV channel. We are still working on developing a similar correction for the FUV channel. The trends in the long-wavelength end of the FUV range indicate that an additional correction is required. This work is in progress for the final version of the data product.

5. UNCERTAINTY ESTIMATES

5.1. Calibration Uncertainty

SOLSTICE was calibrated at NIST SURF III (Arp et al. 2000) before launch. The details of the ground calibration and uncertainty are described in McClintock et al. (2005b). Figure 32 shows the summary of the uncertainty in the final calibration. All uncertainty estimates described in this document are k=1.

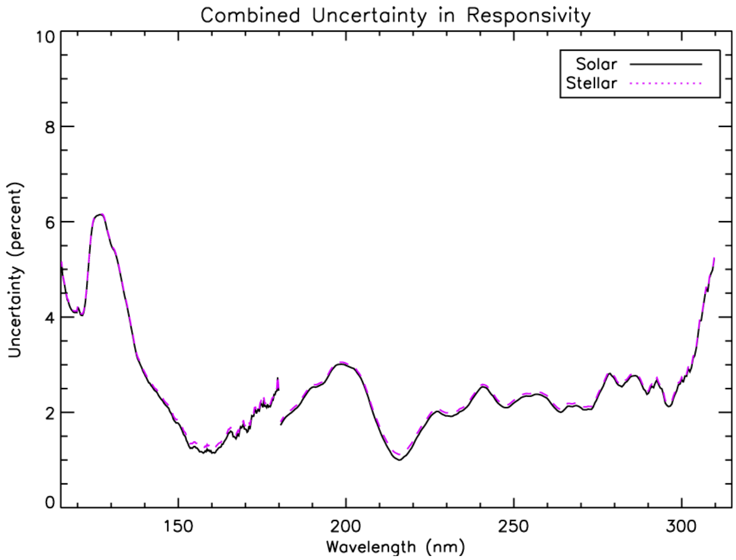

Figure 32. SOLSTICE calibration uncertainty summary (McClintock et al. 2005b).

5.2. Measurement Uncertainty

The measurement uncertainty in the SOLSTICE level 3 data products are primarily due to the statistical uncertainty of the photon-counting system. Figure 33 shows the uncertainty of the 24-hour average of the 1-nm binned SSI. In the FUV, it is between 0.2% and 0.5% for most wavelengths. The counting statistics are better in the MUV by about an order of magnitude: 0.01% to 0.05%.

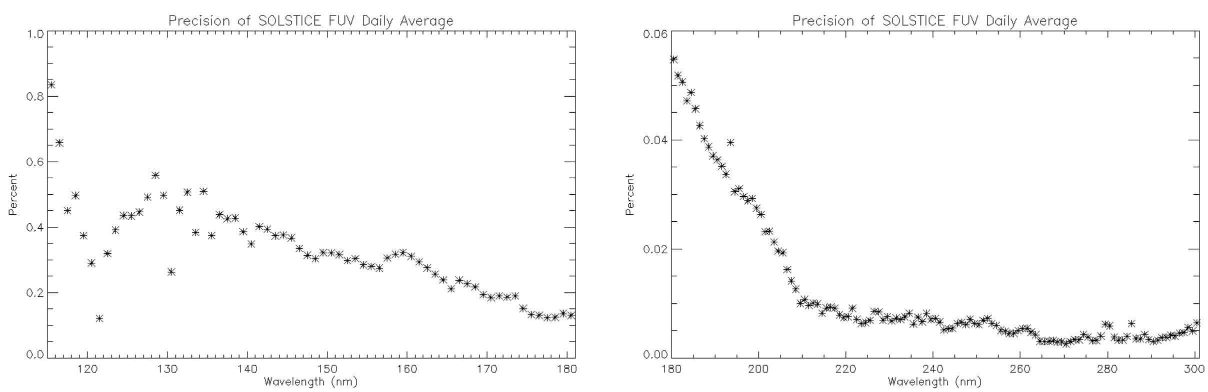

Figure 33. Statistical uncertainty of the daily averaged 1nm binned level 3 irradiance.

5.3. Degradation Uncertainty

The uncertainty in the degradation correction is determined by the uncertainty in the exponential fits to the stellar and haystack observations. The formal uncertainty in the fit parameters yield a trend uncertainty of about 0.35% per year.

- Stellar correction ~0.2%/year

- Haystack correction ~0.2%/year
- ABComparison correction (SOLSTICE A MUV Only) ~0.2%/year
- Combined uncertainty: ~0.35%/year

The correction for the one-day hit and the “spike” correction after the six-month safehold contribute less than a percent. The long-term effects of these two corrections are captured in the calibration observations, so they are not bookkept separately. Data after the vacation has a fraction of a percent additional calibration uncertainty.

The requirement levied on the SOLSTICE instrument by the original ATBD was 0.5% per year, so we are meeting all requirements.

6. VALIDATION

6.1. Validation Method/Description

The SOLSTICE SSI results can be compared to other measurements and models for validating the calibration and trends.

6.2. Comparison with other measurements

Since 2008, there have been three major missions observing SSI in the SOLSTICE wavelength range. On the Picard mission, the PREcision Monitoring Sensor (PREMOS, Cessateur et al. 2016) filter radiometer makes measurements near 215 nm. The SOLAR mission on the International Space Station includes a SOLar SPECtrometer (SOLSPEC, Thuillier 2009). The Total and Spectral Irradiance Sensors (TSIS-1) includes a prism spectrometer that is a second generation version of SORCE SIM. We will compare SOLSTICE observations to each of these in this section.

There are also the solar UV irradiance observations that overlap with SOLSTICE from SORCE SIM, UARS SOLSTICE, UARS SUSIM, TIMED Solar EUV Experiment (SEE), Probas-2 LYRA, OMI, and GOES EUVS. As these measurements have used SORCE SOLSTICE to validate their own time series, we don’t consider them fully independent of SORCE SOLSTICE and thus don’t show those comparisons here.

6.2.1. PREMOS

After convolving the PREMOS instrument profile with the SOLSTICE high resolution spectrum, we can compare the SSI measurements over the Picard mission. Figures 34 and 35 show the time series of irradiances and the ratio to the SOLSTICE observations over the same bandpass and time period (fig. 13 from Cessateur et al. 2016). Two PREMOS channels are shown, 210 nm and 215 nm. In both cases the calibration and variation are well within 1%. There were only a few years of observations from PREMOS, but it is a valuable validation of the short term measurement from SOLSTICE.

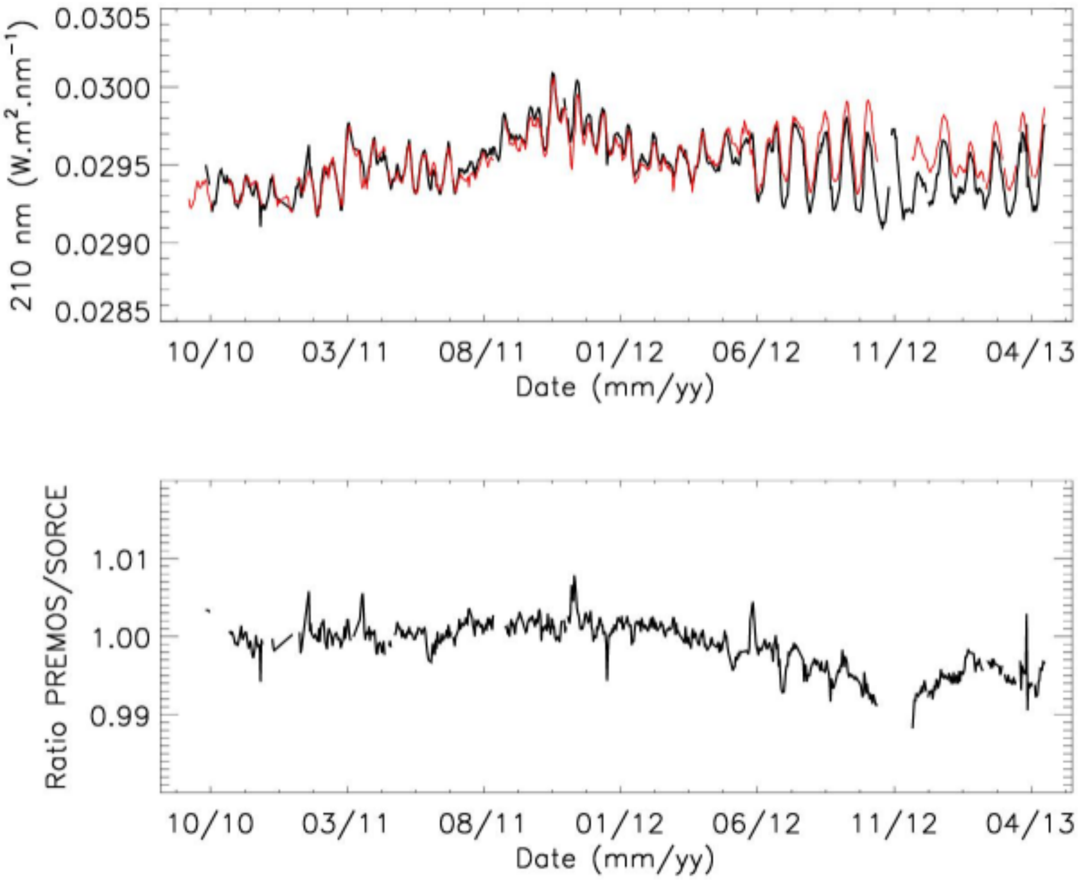

Figure 34. Comparison of SOLSTICE and PREMOS at 210 nm (Figure 13 of Cessateur et al. 2016).

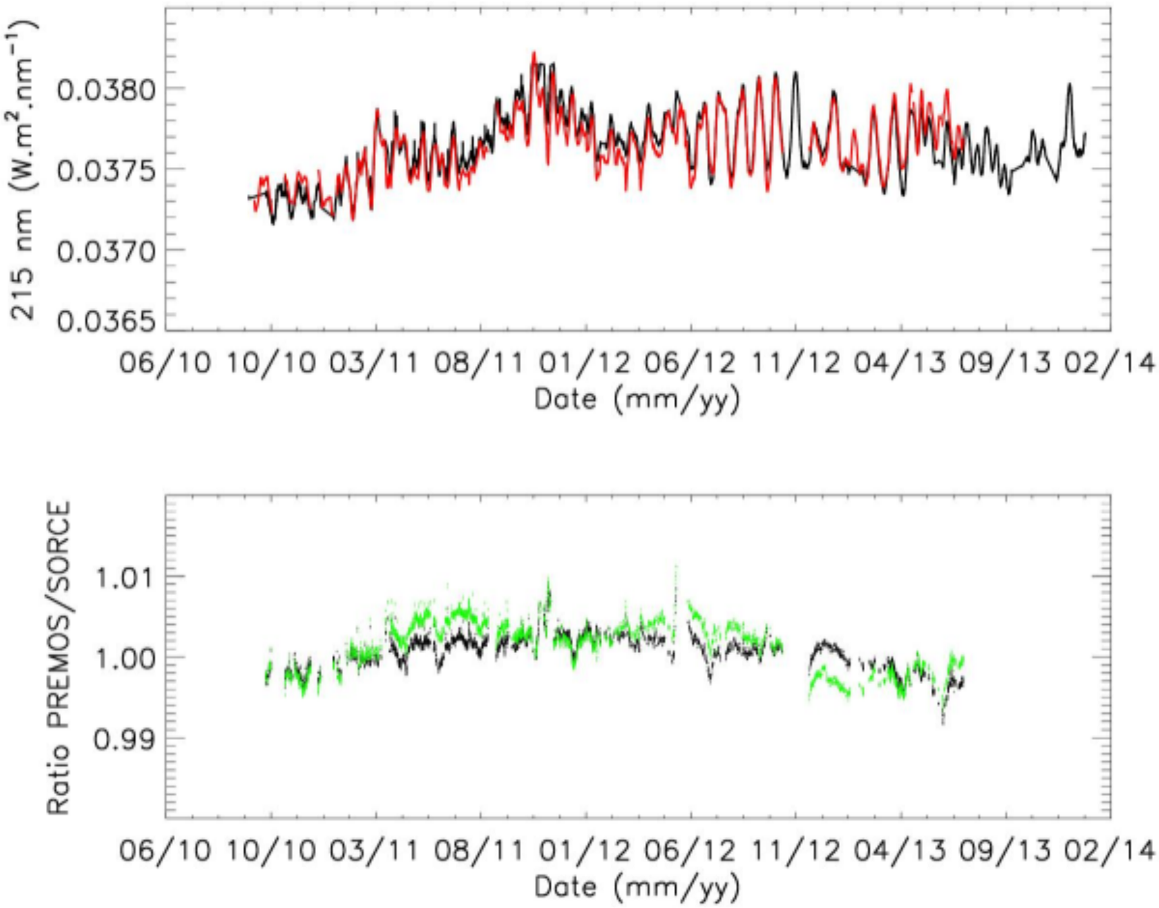

Figure 35. Comparison with PREMOS at 215 nm. (Figure 14 of Cessateur et al. 2016). Version 15 SOLSTICE is shown in black. The green curve is the ratio to version 13.

6.2.2. SOLSPEC

The SOLar SPECrum (SOLSPEC, Thuillier et al. 2009) is one of three instruments in the ESA SOLAR mission on board the International Space Station. It is a double monochrometer and was calibrated using a blackbody at the PTB in Germany. The published uncertainty in this wavelength range is about 2% (Thuillier et al. 2009). The first-light spectrum is the average over the month of April 2008. This time period was at solar minimum, so the intrinsic variation in the signal is probably less than 1%. In comparison to SOLSTICE, April 2008 is five years into its mission. The uncertainty in calibration for each instrument, plus the uncertainty of the SOLSTICE degradation over five years (Section 5.3) of 1.5% are all independent sources of uncertainty and can be added in quadrature. The uncertainty in the ratio is therefore about 4%. This ratio with the uncertainty was published in Snow et al. (2018) and is shown in Figure 36.

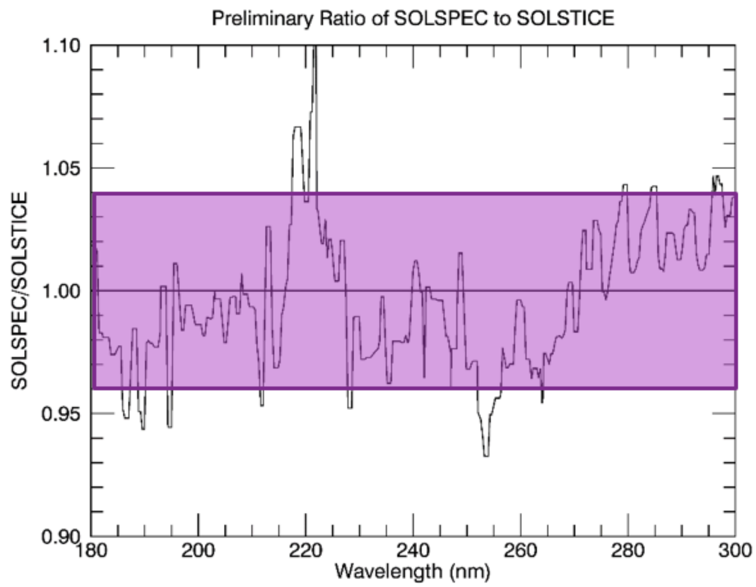

Figure 36. Ratio of SOLAR/SOLSPEC to SORCE/SOLSTICE in April 2008. The shaded area indicates the 1 sigma calibration uncertainty of SOLSTICE (~4%) Figure 4 of Snow et al. (2018).

The long-term calibration of SOLSPEC is uncertain. The design of the instrument called for regular observations of lamps to maintain the calibration. These lamps failed early in the mission, so the SOLSPEC team has had to make several assumptions in order to correct their data. The most recent version of SOLSPEC calibration is described in Meftah et al. (2020).

6.2.3. TSIS-1 SIM

The Total and Spectral Irradiance Sensors (TSIS-1) Spectral Irradiance Monitor (SIM) is the next generation prism spectrometer calibrated and operated by LASP. It is currently onboard the International Space Station and taking daily data. In order to compare the TSIS-1 SIM with SOLSTICE, we convolved the SOLSTICE spectrum with the SIM instrument function as shown in Figure 37. A prism has a smoothly varying spectral resolution, so a quantitative comparison requires that this step be done as accurately as possible

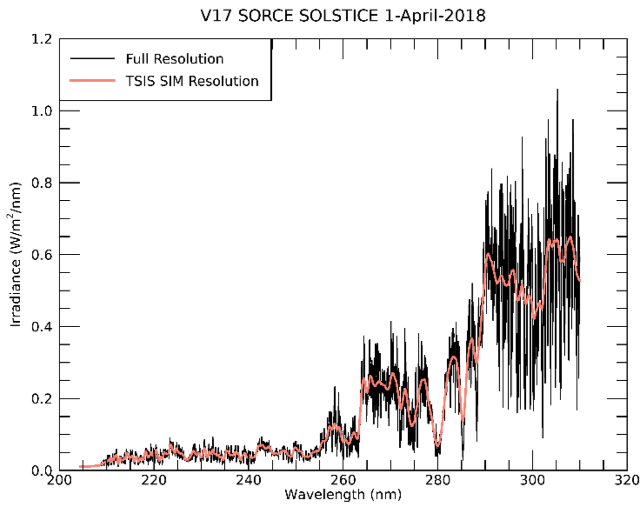

Figure 37. SOLSTICE MUV spectrum convolved with the TSIS-1 SIM instrument profile.

Figure 38 shows the SOLSTICE and TSIS-1 SIM spectra overplotted on an absolute scale. Figure 39 shows the ratio of the two spectra. Recalling that the uncertainty in the SOLSTICE degradation correction is 0.35%/year, this comparison 15 years after the launch of SORCE is excellent agreement. TSIS-1 SIM had an extensive ground calibration, and its uncertainty is 1% or less throughout the wavelength range that overlaps SOLSTICE. Therefore the expected 1-sigma uncertainty in the ratio is about 4%.

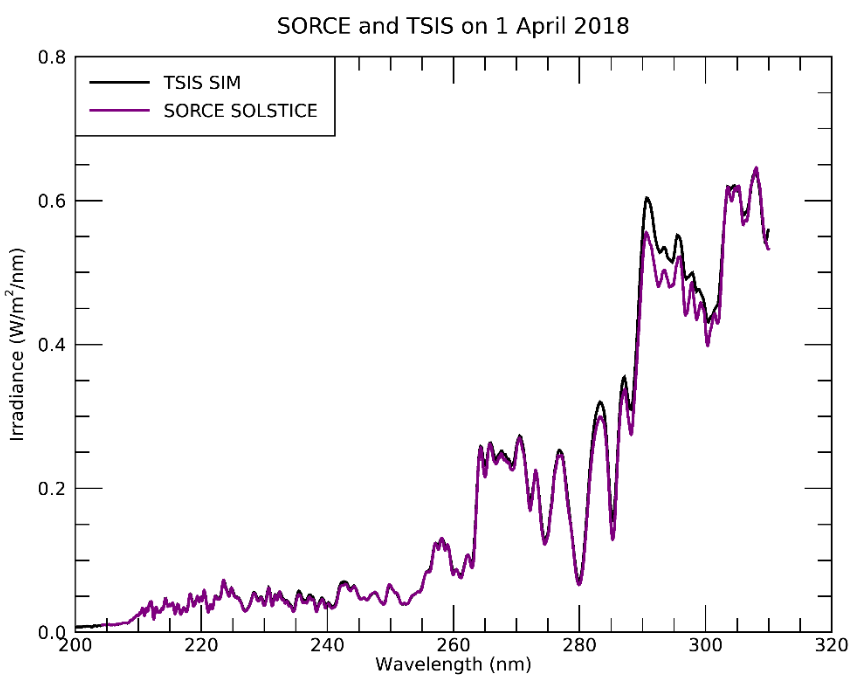

Figure 38. TSIS-1 SIM and SORCE SOLSTICE calibrated irradiances on 1 April 2018, shortly after SIM became operational.

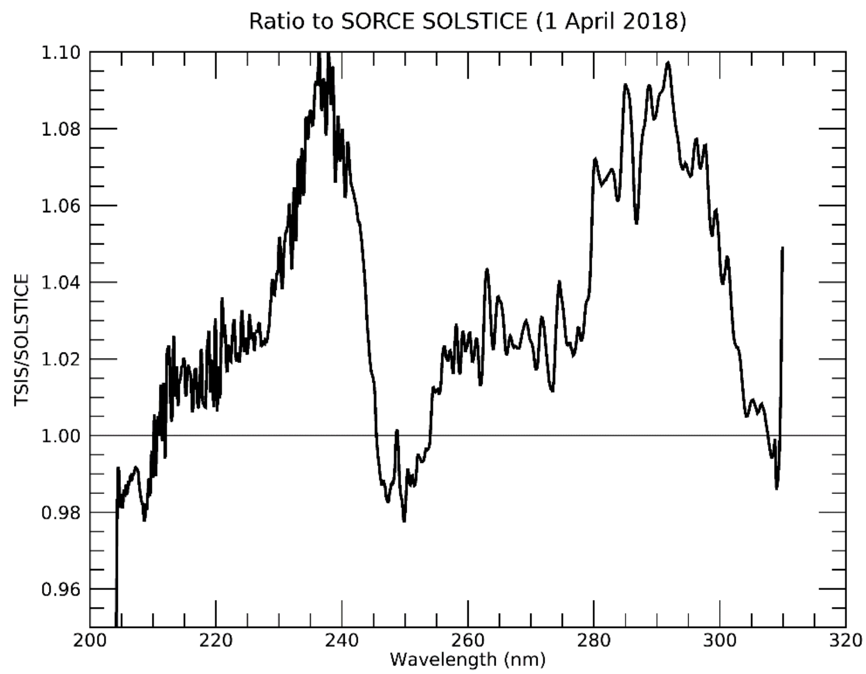

Figure 39. Ratio of SORCE/SOLSTICE (v17) and TSIS-1/SIM (v3) on 1-April-2018.

The shape as a function of wavelength may help resolve some inconsistencies in the SOLSTICE degradation analysis. In particular, the haystack and DO-Op offpoints do not agree well above 280 nm. The TSIS ratio indicates that the DO-Op measurements are more reliable. The SOLSTICE irradiances are systematically lower than TSIS, so the degradation function is not capturing enough degradation, perhaps. Considering that the SORCE SOLSTICE stability is estimated at 0.35%/year, these SOLSTICE and TSIS-1 differences are mostly within 1-sigma 6% trending uncertainty for SOLSTICE over its 17-year mission.

6.3. Comparison with SSI models

There are two primary SSI models used by the community, NRLSSI2 (Coddington et al. 2016) and SATIRE-S (Yeo et al. 2014). Both models are calibrated to match SOLSTICE in absolute scale, so it only makes sense to compare the relative variability on short and long time scales. Figure 40 shows a comparison of rotational variability between SOLSTICE and the two models. Since NRLSSI2 uses SOLSTICE to define its rotational variation magnitude, it is not surprising that there is good agreement. SATIRE-S uses a different method to determine variability. Below about 160 nm, SATIRE-S shows larger rotational variability than SOLSTICE. Above 160 nm, it is in fairly good agreement.

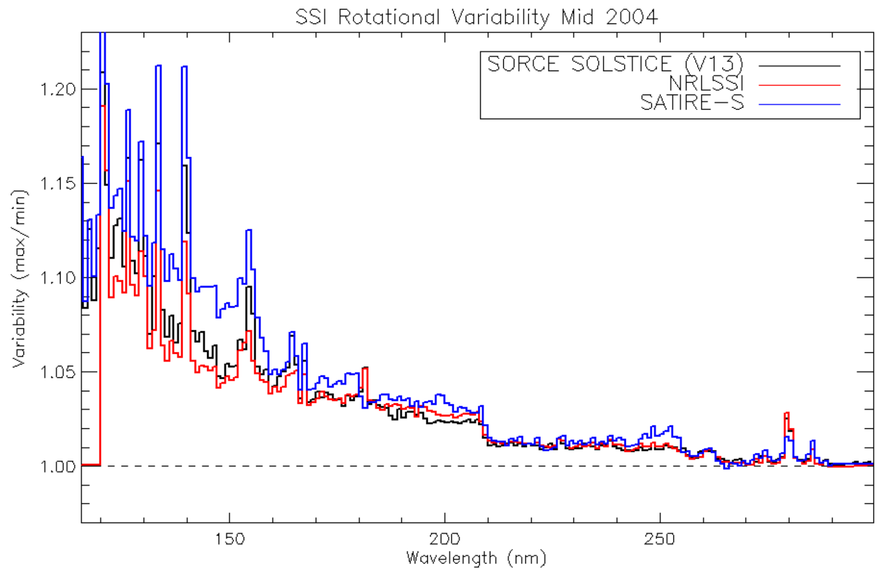

Figure 40. Rotational variability in SOLSTICE, NRLSSI2, and SATIRE-S.

Solar cycle variability is a primary measurement of SORCE SOLSTICE. Figure 41 shows the comparison of the FUV band (left) for the decline of solar cycle 23 and the rise of solar cycle 24 for both SOLSTICE and the NRLSSI2 model. SC 23 is systematically higher by several percent, but SC 24 agrees very closely. The right panel of Figure 41 shows the MUV variability. Considering that the variability in this part of the spectrum is only a few percent, a disagreement of a percent is significant. The measurements during the decline of SC 23 do not really agree with the proxy model. The SOLSTICE team has struggled to understand the degradation in the early part of the mission, and work is continuing. In particular, the long wavelength part of the spectrum is very difficult to correct. The signal-to-noise of the stellar measurements is extremely poor, and there is an inconsistency between the haystack and DO-Op observations (Section 4.3.1.3).

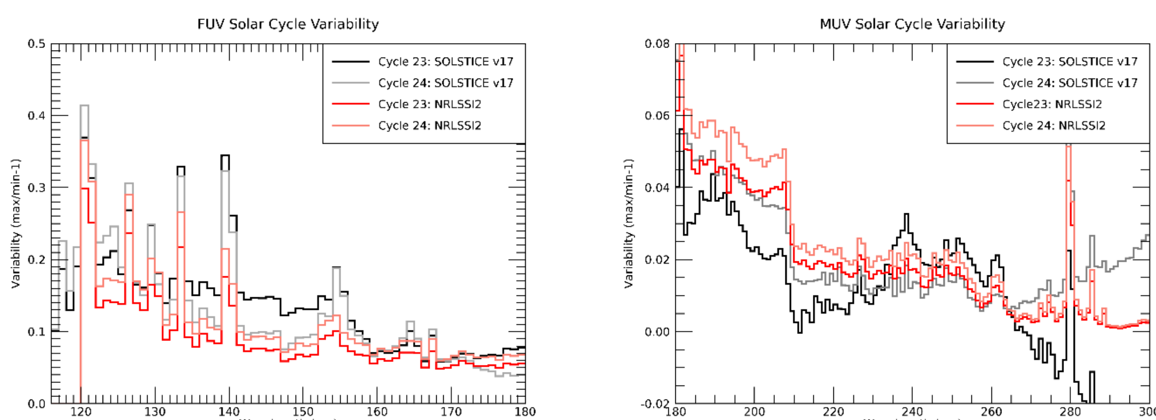

Figure 41. Solar cycle variability compared to NRLSSI2 for version 17 SOLSTICE.

The time series of an important wavelength band (220-240 nm) is shown in Figure 42. The left panel shows the large disagreement between models and other measurements relative to the SORCE instruments. The latest data version (v17) shows much better agreement. Due to the shape of the solar spectrum, this band is weighted towards the longer wavelengths, which happen to agree better (see Figure 41).

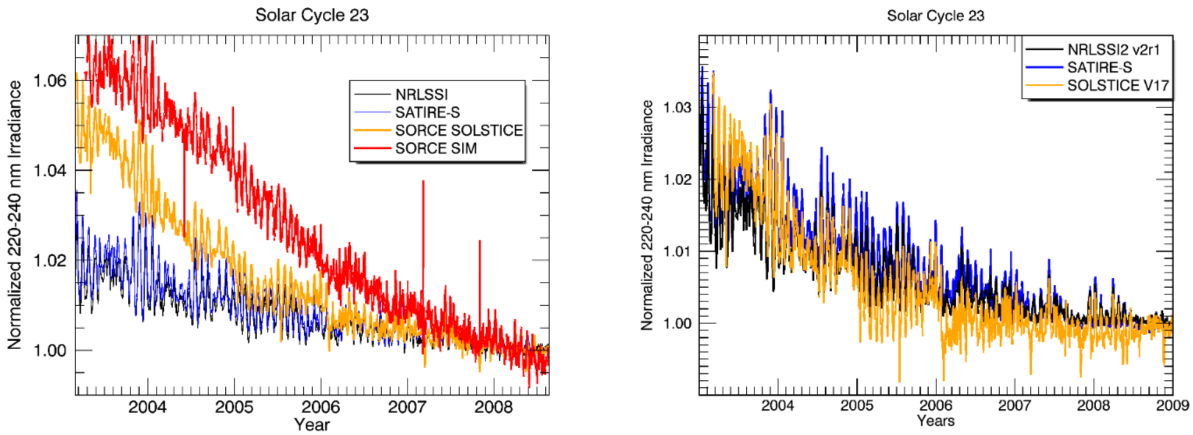

Figure 42. Comparison of SOLSTICE solar cycle 23 variation in the 220-240 nm band. The panel on the left shows version 13 of SOLSTICE data (from Ermolli et al. 2013). Version 17 data are shown on the right.

7. DATA PRODUCT DESCRIPTION

7.1. Overview

The SORCE project uses the data level definitions that are consistent with NASA Earth Science conventions as described in the *Earth Science Reference Handbook – A guide to NASA's Earth Science Program and Earth Observing Satellite Missions* [available via *http://eospso.nasa.gov/publications/56*]. Data products are archived and made available to the public at the NASA Goddard Earth Sciences Data and Information Services Center (GES DISC).

7.2. Data Level Definitions

The results from the various processing levels are stored in separate database tables. The data from the lower levels are used as inputs when processing the higher data levels. Table 7.1 provides information about each level for the SORCE SOLSTICE instrument.
Only the fully calibrated Level 3 data product is routinely made available to the scientific community and general public. All levels, however are archived at the NASA GES DISC and made available upon special request.

7.3. Level 2 Products

Level 2 data products are the lowest level that are in physically meaningful units (e.g. wavelength in nm and irradiance in $W/m^2/nm$). These are at the full time cadence and spectral resolution of the instrument. A slightly higher level data product with the degradation correction applied, but no time averaging is used for internal analysis.

There are two public data products that qualify as level 2: the MgII index and the Lyman-alpha profile. Both of these observations are taken at high cadence several times per day. During the prime mission, they each were observed continually over a full orbit. In DO-Op mode, they are still observed several times per orbit.

The Lyman-alpha scan is a 64-step scan over the line profile with 1s integration times. The full profile is measured about once per minute. This data product has been created by special request in the past, but we have released the full mission scans with version 18.

The MgII index scan includes a scan over the core and wing regions at the beginning and end of one orbit per day, and then high cadence observations of just the core region for the rest of that orbit. The wing reference measurements are slowly varying compared to the core, so they do not need to be sampled at high cadence. The resulting time resolution of the core-to-wing ratio is 47 s. The core measurements are at higher spectral sampling than normal (9 DN steps rather than the standard 27 DN steps). The higher sampling was found to improve the signal to noise ratio of the core measurement (Snow & McClintock, 2005). The version 18 MgII index will use the algorithm described in Snow et al. (2019).

7.4. Level 3 Products

There are two level 3 SOLSTICE data products. Both are constructed from a daily average of all SolarNormalScan data. For each 24 hour period, all of the level 2 spectra are aggregated and fit with a basis spline function (degradation-corrected irradiance vs wavelength). The data product described in the original ATBD is created by numerically integrating this spline over 1 nm intervals. A newer level 3 data product is created by evaluating this spline on a regular wavelength grid with 0.025 nm spacing. The "high resolution" spectrum approximates the wavelength sampling of the raw data. It is available as a NetCDF file (one per year) from the SORCE web page.

7.5. Practical Algorithm Considerations

The SORCE data processing system accesses calibration data through look-up tables for most needs instead of running the full instrument model. This approach considerably improves ease in analysis and increases the processing speed without affecting the accuracy of the processed data. The individual calibration data look-up tables are stored in separate database tables. Additionally, SORCE instruments and spacecraft telemetry metadata as well as the planning and scheduling data are also stored in database tables. All of these tables are archived at the NASA GES DISC.

8. PRODUCTION of SCIENCE DATA

8.1. Overview

All science data production and management activities are provided by the LASP SORCE Science Data System, which resides at LASP in Boulder, Colorado. The SORCE Science Data System consists of both the hardware and software components necessary to capture, manage, process, analyze, validate, and distribute all science data products.

At the core of the system resides a commercial relational database system, in which all telemetry, calibration data, scientific data products, and ancillary information are stored. All data are stored in the database as individual time-referenced points to provide direct and rapid access to each datum received from the spacecraft or instruments or subsequently processed. Certain file cataloging and archiving activities are also required to manage these data, for instance, design documentation and raw telemetry data as received from the ground stations following spacecraft contacts.

The data processing and calibration data management software, written in the Java programming language, are tightly coupled with the SORCE project database, in which all data sources and products are stored. The data processing component of the system interacts directly with the time-referenced data as stored in the database in order to provide efficient data utilization. Level 3 Irradiance data products are queried from the database and written out to ASCII data files which include full product metadata in the header of each file and are made available to the public.

8.2. Data Management

All project data will be managed within a commercial relational database management system (DBMS). This system will maintain, under configuration control, all software, raw instrument and spacecraft data, engineering data products, science data products, calibration data, operations plans, and ancillary data. Data security will be maintained using standard firewall and system security techniques, while integrity will be guaranteed by employing backup/recovery capabilities and utilizing automated sweep systems that are built into modern commercial DBMS products.

8.3. Data Filtering

In order to ensure the quality of the data products, we must first filter out data that do not meet strict quality standards. For example, data collected while the spacecraft is flying over what is known as the South Atlantic Anomaly (SAA) is contaminated by counts produced by high energy particle impacts on the detector, and therefore have to be excluded from data processing. In addition, during an observation only data collected within a narrow FOV are used to produce the final data products.

8.4. Data Processing Flow Chart

The SORCE SOLSTICE data are processed from raw units of counts per second into irradiance values (Level 2 product), and then calibrated for instrument degradation and adjusted for a mean distance of 1AU from the Sun. This degradation-corrected L2 product is integrated over 1nm intervals to produce the Level3 irradiance data product.

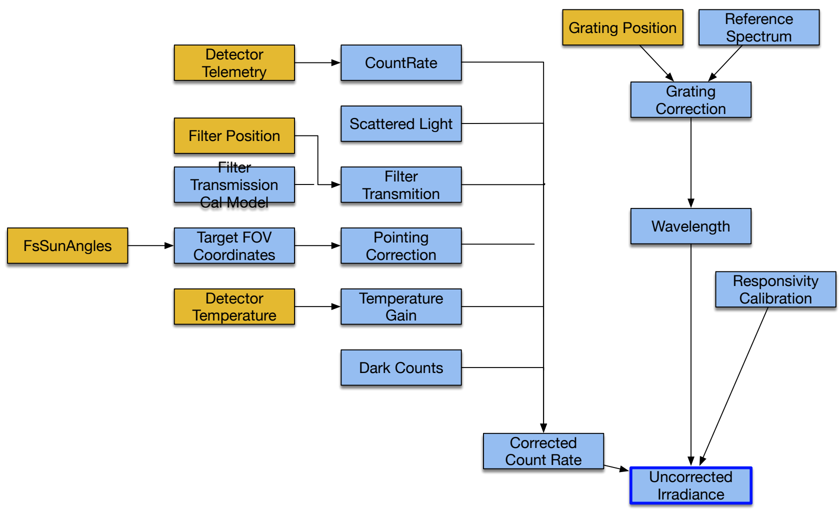

Figure 43. Level 2 processing workflow. Yellow boxes indicate instrument telemetry and blue boxes indicate derived products.

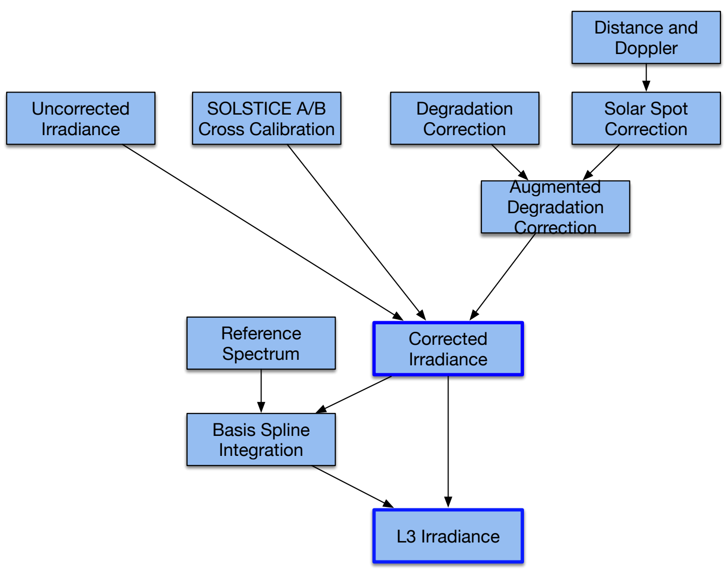

Figure 43. L2 to L3 data processing workflow.

8.5. Data Structure

The Level 3 data product is the science -quality data product made available to the public. The following table lists the variables in the L3 SOLSTICE data product.

Table 8.1. SOLSTICE Level 3 Data Product Columns

Variable	Description	Type	Range
NOMINAL_DATE_ YYYYMMDD	Date as Year-Month-Day number	double	20030302 - 20200225
NOMINAL_DATE_JDN	Date as Julian Day	double	2452700 - 2458904
MIN_WAVELENGTH	Bandpass minimum wavelength (nm)	double	115-309nm

MAX_WAVELENGTH	Bandpass maximum wavelength (nm)	double	116-310nm
IRRADIANCE	Daily average Irradiance ($W/m^2/nm$)	double	1.32E-5 – 6.78E-1
IRRADIANCE_UNCERTAINTY	Irradiance uncertainty (relative in %)	double	4.42E-7 – 2.77E-2
DATA_VERSION	Data product version number	Int	Positive integer
INSTRUMENT_MODE_ID	Instrument mode identifier	Int	7,9,11 or 13

8.6. Software Configuration

The SORCE Science Data System processing code is maintained and archived in a version controlled code repository. The code selected for SORCE SOLSTICE data production undergo peer code reviews using collaborative and iterative code review software tools, unit testing, and continuous integration testing as part of a systematic production code release process.

9. Appendix: release notes

10. Bibliography

Arp, U., Friedman, R., Furst, M. L., Makar, S., & Shaw, P.-S. (2000) Metrologia, 37, 357.

Cessateur, G., et al. (2016) Solar irradiance observations with PREMOS filter radiometers on the PICARD mission: in-flight performance and data release, Astronomy & Astrophysics, 588, id A126.

Coddington, O., et al. (2016) A solar irradiance climate data record, Bulletin of the American Meteorological Society, 97, 1265.

Ermolli, I., et al. (2013) Recent variability of the solar spectral irradiance and its impact on climate modelling, Atmospheric Chemistry and Physics, 13, 3945.

McClintock, W., Rottman, G., & Woods, T. (2005a) Solar-stellar irradiance comparison experiment II (SOLSTICE II): instrument concept and design, Solar Physics, 230, 225.

McClintock, W., Snow, M., & Woods, T. (2005b) Solar-stellar irradiance comparison experiment II (SOLSTICE II): pre-launch and on-orbit calibrations, Solar Physics, 230, 259.

Meftah, M., et al. (2020) A new version of the SOLAR-ISS spectrum covering the 165-3000 nm spectral region, Solar Physics, 295, 14.

Snow, M. & McClintock, W. (2005) High time cadence solar magnesium II index monitor, Proc. SPIE, 5901, 354.

Snow, M., McClintock, W., Rottman, G., & Woods, T. (2005a) Solar-stellar irradiance comparison experiment II (SOLSTICE II): examination of the solar stellar comparison technique, Solar Physics, 230, 295.

Snow, M., et al. (2005b) The Mg II index from SORCE, Solar Physics, 230, 325.

Snow, M., et al. (2013) A new catalog of ultraviolet stellar spectra for calibration, in *Cross-Calibration of Far UV Spectra of Solar System Objects and the Heliosphere*, E. Quémerais, M. Snow, and R-M. Bonnet (eds), ISSI Scientific Report Series volume 13, pp 191.

Snow, M., et al. (2014) Comparison of magnesium II core-to-wing ratio observations during solar minimum 23/24, Journal of Space Weather and Space Climate, 4, A04.

Snow, M., et al. (2018) Ultraviolet solar spectral irradiance variation on solar cycle timescales, in *Long-term Datasets for the Understanding of Solar and Stellar Magnetic Cycles,* Proceedings of the IAU, IAU Symposium 340, p203.

Snow, M., et al. (2019) A revised magnesium II core-to-wing ratio from SORCE SOLSTICE, Earth & Space Science, 11, 2106.

Thuillier, G., Foujols, T., Bolsee, D., et al. (2009) SOLAR/SOLSPEC: scientific objectives, instrument performance and its absolute calibration using a blackbody as primary standard source, Solar Physics, 257, 185.

Yeo, K., Krivova, N., Solanki, S., & Glassmeier, K. (2014) Reconstruction of total and spectral solar irradiance from 1974 to 2013 based on KPVT, SoHO/MDI, and SDO/HMI observations, Astronomy & Astrophysics, 570, A85.